

EUROVOLC

European Network of Observatories and Research Infrastructure for Volcanology

Deliverable Report

D12.2 Quantitative hazard assessment at test volcanoes

Work Package:	<i>Exploitation of tools for hazard assessment and risk management</i>	
Work Package number:	<i>12</i>	
Work Package leader:	<i>Laura Sandri</i>	
Task (Activity) name:	<i>Exploitation of tools for hazard assessment and risk management</i>	
Task number:	<i>1</i>	
Responsible Activity leader:	<i>Laura Sandri</i>	
Lead beneficiary:	<i>INGV</i>	
Author(s)	<i>Silvia Massaro, Eduardo Rossi, Fabio Dioguardi, Costanza Bonadonna, Laura Sandri, Sara Barsotti, Adelina Geyer, Emmie Bonilauri, Andrew Harris, Jacopo Selva, Antonio Costa, Roberto Moretti, Jean-Christophe Komorowski, Giancarlo Tamburello, Severine Moune, David Jessop, Tomaso Esposti Ongaro, Yoann Legendre, Augusto Neri, Diana Jiménez</i>	
Type of Deliverable:	Report <input checked="" type="checkbox"/>	Demonstrator <input type="checkbox"/>
	Prototype <input type="checkbox"/>	Other <input type="checkbox"/>
Dissemination level:	Public <input checked="" type="checkbox"/>	Restricted Designated Group <input type="checkbox"/>
	Prog. Participants <input type="checkbox"/>	Confidential (consortium) <input type="checkbox"/>

Contents

Summary	2
Introduction	2
1 – Application of previously existing hazard tools to La Soufrière de Guadeloupe	4
1.1 Validation of DISGAS model at La Soufrière de Guadeloupe to simulate volcanic gas dispersal .	4
1.1.1 Introduction	4
1.1.2 Methodology.....	4
1.1.3 Results from testing the model performance.....	5
1.2 Application of Great Balls of Fire model at La Soufrière de Guadeloupe to quantify hazard from volcanic ballistics.....	8
1.2.1 Introduction	8
1.2.2 Methodology.....	8
1.2.3 Sensitivity analyses	10
1.2.4 Hazard results and analysis of the potential impacts	11
1.3 Application of the PDAC model at La Soufrière de Guadeloupe to quantify hazards from pyroclastic currents resulting from the collapse of explosive Sub-Plinian and Plinian eruption columns, case study of the 1530 C.E. eruption at La Soufrière de Guadeloupe	13
1.3.1 Introduction	13
1.3.2 Methods.....	13
1.3.3 Results.....	15
1.3.4 Conclusions	17
2 – Application of previously existing hazard and risk tools to other volcanoes.....	19
2.1 Application of HASSET tool to San Miguel, Salvador	19
2.1.1 Introduction and context	19
2.1.2 Scientific objectives.....	20
2.1.3 Methodology.....	20
2.1.4 Preliminary results	21
2.2 Application of CALPUFF model to Bárðarbunga eruption in 2014-2015, Iceland, to quantify gas hazard	22
2.3 GIS-based risk analysis for evacuation modelling at Stromboli.....	25
2.3.1. Introduction	25
2.3.2. Methodology.....	26
2.3.3. Modelling results	26
2.3.4. Considerations	28
3 – Development of new open tools for volcanic hazard assessment	31
3.1 VIGIL: an automatized probabilistic volcanic gas dispersion model.....	31
References	32
Appendix A: Links to concrete results.....	38

Summary

This report summarizes the activity carried out in Task 12.1 of project EUROVOLC.

In **section 1** we report on the applications carried out at the originally-identified test volcano of La Soufrière de Guadeloupe. In particular, we have validated, against field measurements, the skill of the DISGAS model in reproducing the gas concentration data in a hazard perspective (section 1.1); further, we have calibrated and applied the Great Balls of Fire model to quantify the hazard from ballistic impact of the typical roofs on the island (section 1.2). Finally, we report on application of the PDAC model to quantify the hazard of pyroclastic density currents from collapse of explosive Sub-Plinian to Plinian eruption columns.

In **section 2** we report on other hazard assessments carried out within EUROVOLC Task 12.1, at other target volcanoes. In particular, we report on the application of the HASSET model to San Miguel volcano (El Salvador) in section 2.1; in section 2.2 we report on the study to quantify volcanic SO₂ hazard through the CALPUFF model, in the aftermath of the Bárðarbunga eruption in 2014-2015; in section 2.3 we show the development of a new method based on Geographical Information System methodology to generate large-scale and individual building evacuation plans for the study case of Stromboli.

Finally, in **section 3** we describe a new tool, developed within EUROVOLC Task 12.1, to quantify the probabilistic hazard from volcanic gases through an automated procedure.

We remark that most of the applications discussed here have been published in peer-reviewed scientific journals (sections 1.1, 2.2) or are in the review process (sections 1.2 and 3.1).

Introduction

This deliverable stems from the work carried out in the first year of the EUROVOLC project, in which we collected and catalogued the open-use models and codes that concur to the quantification of volcanic hazard and that are available from the literature. The software catalogue (Deliverable D12.1) was created and it is currently hosted at: <http://193.206.223.51:8088/index.php/softwarelist>. The other goal of Task 12.1 was to select the most suitable hazard tools, among those listed, and apply them to the test volcano of La Soufrière de Guadeloupe in the French island of Guadeloupe (Lesser Antilles) (**Figure 1**).



Figure 1: Location map of La Soufrière de Guadeloupe in the French island of Guadeloupe (Lesser Antilles) and San Miguel (El Salvador) volcanoes.

In this perspective, we selected three of the most likely hazardous phenomena that might accompany the present activity (i.e., gas hazard due to the current gas dispersal from the active fumaroles) and/or the most likely explosive scenario at La Soufrière de Guadeloupe amongst those elaborated by the civil authorities in collaboration with the Observatoire Volcanologique et Sismologique de Guadeloupe, i.e. ballistic impact as well as the modelling of pyroclastic density currents from collapse of explosive Sub-Plinian to Plinian eruption columns.

To quantify the gas hazard, a fundamental step is the model validation. For this, it is necessary to carry out a quantitative check on the skill of the chosen model to reproduce gas concentration in a hazard perspective, that is, considering the epistemic uncertainty related to the gas fluxes at the sources and the wind field. In this view, the

first work presented in this deliverable (Section 1.1) illustrates the application of the DISGAS model (Costa & Macedonio, 2016), selected from the D12.1 catalogue, to quantitatively validate its performance in hazard assessment.

To quantify ballistic-impact hazard associated with the most likely explosive scenario at La Soufrière de Guadeloupe (including phreatic, Vulcanian and Strombolian eruptions) we selected the Great Balls of Fire model (Biass et al, 2016) from D12.1 catalogue. Then, we have applied it considering as possible source the summit dome of La Soufrière, including the uncertainty on the vent position in case of explosion, and the variability related to uncertain eruption source parameters (Section 1.2). Also, the effect of wind was quantified, although it turns out to be negligible in the outcoming hazard assessment.

To quantify the hazard associated with the emplacement of pyroclastic density currents formed during eruptive scenarios that involve the collapse of explosive Sub-Plinian to Plinian eruption columns, such as the case study eruption of 1530 C.E. (Boudon et al., 2008; Komorowski et al., 2008), we have used the three-dimensional, multiphase flow model PDAC (i.e. Pyroclastic Dispersal Analysis Code; Neri et al. 2003; Esposti Ongaro et al. 2007; Carcano et al. 2013) from the D12.1 catalogue. Then, we have applied it considering as possible source the summit area of La Soufrière using eruption source parameters (Section 1.2) as detailed by Komorowski et al., (2008), Boudon et al., (2008), and Spence et al., (2008).

In addition to these applications to the test volcano of La Soufrière de Guadeloupe, we also report on applications to quantify hazard related to volcanic activity at other target volcanoes, i.e. San Miguel (El Salvador, **Fig. 1**), Bárðarbunga (Iceland, **Fig. 2**) and Stromboli (Italy, **Fig. 2**).

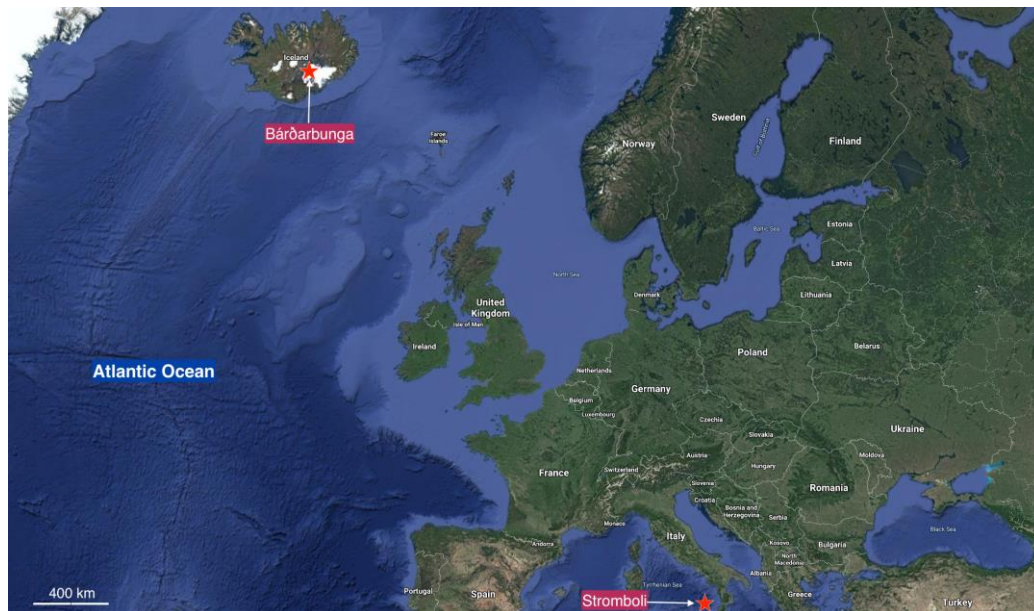


Figure 2: Location map of Stromboli (Italy) and Bárðarbunga (Iceland) volcanoes.

In the framework of the E-THA project (e-Tools for short-term volcanic Hazard Assessment) submitted to the 1st EUROVOLC Transnational Access Call by Dr. Diana Jimenez from the University of El Salvador, the HASSET short term e-tool (Sobradelo et al. 2013, listed in D12.1) was used to estimate the probability of occurrence of a particular eruptive scenario combining monitoring data with information on past eruptions and unrest episodes.

For the case study of Bárðarbunga, we focus on the quantification of volcanic SO₂ hazard after the 2014-15 eruption, through the CALPUFF model (Barsotti et al. 2008; Barsotti and Neri 2008) listed in D12.1.

For the case study of Stromboli, we developed a new method based on the Geographical Information System (GIS) methodology to generate large-scale and individual building evacuation plans.

Finally, in the application of DISGAS model, we developed a new code, called VIGIL, consisting of a suite of automatized python routines that a user can call to retrieve meteorological data, run DISGAS model, postprocess the simulations and produce hazard and probability maps. This work was done within EUROVOLC Task 12.1 and contributed to enlarge the collection of hazard tools, codes and models listed in D12.1.

1 – Application of previously existing hazard tools to La Soufrière de Guadeloupe

1.1 Validation of DISGAS model at La Soufrière de Guadeloupe to simulate volcanic gas dispersal

1.1.1 Introduction

In this study, we provided some prototypal tests aimed to validate the modelling of gas dispersal from a hazard perspective at La Soufrière de Guadeloupe volcano (**Fig. 1 & 3a**) which was chosen as test case for a variety of reasons: first, it is a volcano showing some signs of unrest, and it is very useful and interesting to contribute to quantify the hazard in this situation; secondly, La Soufrière has not received much attention in previous recent EU projects, even if it is one of the most active gas emitters in the Lesser Antilles.

We tested the capability DISGAS-2.0 (Dispersion of GASes; Costa and Macedonio, 2016), i.e., its ability in reproducing the correct order of magnitude and variability (e.g., Tierz et al., 2016) of gas concentrations, focussing on the distribution of CO₂ and H₂S discharged from the three main fumarolic sources at the summit (*Tarissan*, TAS; *Cratère Sud*, CS; *Gouffre 1956*, G56) in the period March-April 2017.

The strategy was to run the model on different wind models and/or Digital Elevation Models (DEMs) and varying the resolution of the computational grid, and see how much the output concentrations are affected. To do this, we implemented a new version of the DISGAS code (within a Python environment) which is able to automatically:

- retrieve meteorological data from the ERA5 reanalysis dataset (Copernicus Climate Change Service, 2017) and process them to obtain weather data usable by DISGAS;
- process meteorological data from weather stations in the computational domain;
- randomly locate source emissions from a vent probability map;
- randomly select the emission rate of the sources from a given dataset of possible emission rates;
- perform the simulations with DISGAS and its post-processing.

The results of this study are included in a recently accepted paper: Massaro, S., Dioguardi, F., Sandri, L., Tamburello, G., Selva, J., Moune, S., Jessop, D.E., Moretti, R., Komorowski, J.-C., Costa, A., 2021 “*Testing gas dispersion modelling: A case study at La Soufrière volcano (Guadeloupe, Lesser Antilles)*”, *Journal of Volcanology and Geothermal Research*, 417, 107312, <https://doi.org/10.1016/j.jvolgeores.2021.107312>. See the appendix for a picture of the front cover (**Figure A.1**).

1.1.2 Methodology

The passive advection and diffusion of the gas species emitted by the fumaroles at La Soufrière was carried out by using the Eulerian DISGAS-2.0 (Costa and Macedonio, 2016). The input data in the coupled Diagnostic Wind Model (DWM) include topography, terrain roughness, meteorological data, atmospheric stability information, and gas flow rates from the sources.

In our case, the model inputs at sources are the H₂O fluxes, while the outputs are represented by 2D grid maps of H₂O concentrations dispersed over the topography at different timesteps and levels in the atmosphere. The H₂O concentration outputs are then converted in CO₂ and H₂S concentration (ppm) by using the molar ratios CO₂/H₂O and H₂S/H₂O (Allard et al., 2014; Tamburello et al., 2019).

The computational domain was extended over an area of 9 km² on the volcano and 500 m vertically above the ground (**Fig. 3b**) and discretized by a 200 × 200 cells grid with a horizontal resolution of 15 m and a vertical grid spacing, finer near the surface (from 1 m) and coarser towards the top (up to 250 m), chosen as a good compromise between the accuracy of outputs and computational costs.

In order to understand which input data are more appropriate to obtain a reliable wind field, we carried out two tests by using local meteorological data only (Test 1) and ERA5 reanalysis dataset (Copernicus Climate Change Service, 2017; Test 2) in the DWM (Douglas et al., 1990). Local meteorological data were taken from the Piton Sanner station operated by OVSG-IPGP and located on the summit dome, at ca. 1447 m (**Fig. 1b**). Then, to test

the impact of uncertainty on topography resolution, we checked if the fit between simulation results and observations is the same when using a lower-resolution DEM (25 m; <https://earthexplorer.usgs.gov/>) for the topography (Test 3). In this case, we calculated the wind field by using the data acquired by the local weather station. Finally, to investigate the influence of the computational grid resolution on the model outputs, we reproduced Test 1 by using a 5 m- resolution computational grid (Test 4).

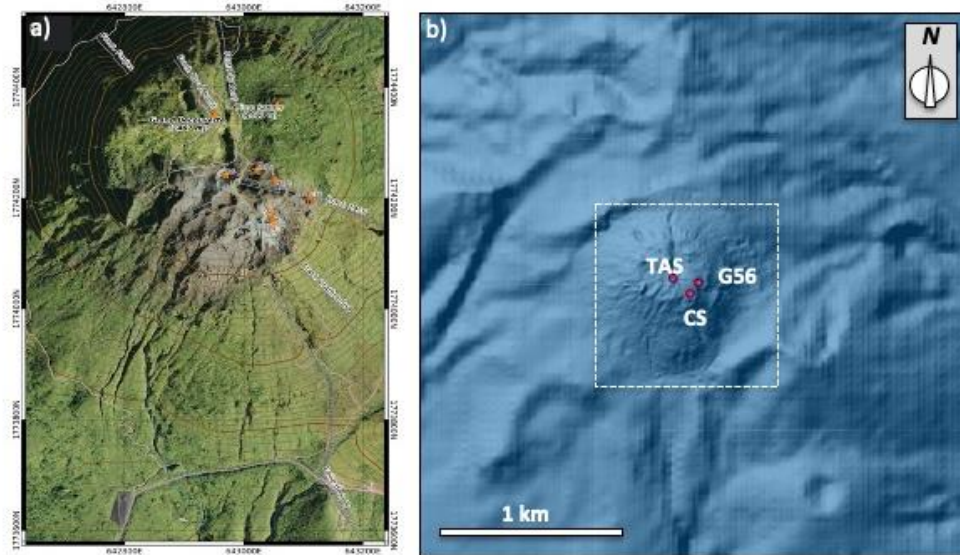


Fig. 3 – a) Map of the summit La Soufrière de Guadeloupe volcano (1467 m asl) showing the main geological features (1956 fractures, Cratère Sud, Fente du Nord, Nord-Ovest, Faujas, and La Ty fault), the location of the active fumaroles (red stars); b) Computational domain (ca. 3 km × 3 km) used for numerical simulations. The grid used is set 200 × 200 (resolution = 15 m) indicating the three active fumaroles TAS, G56 and CS, from *Massaro et al. (2021)*.

From each simulation, we extracted the CO₂ and H₂S concentration at three tracking points on the summit dome, corresponding to the location of the OVSG-IPGP MultiGAS stations (**Fig. 3b**). These points are fixed at 1 m from the ground, so that the observed and simulated concentrations are referred to the same altitude. Since the observations covered 13 days, we provided numerical simulations in two opposite conditions: i) running 11 simulations (each one simulating the entire 13 days of the validation period) varying the daily value of the water vapour flux regardless of each source, in order to catch the natural variability of the gas emission rate shown in the last few years, and ii) running one simulation (simulating the entire 13 days of the validation period) fixing a single water vapour flux for each source. In both cases, the hourly gas concentrations were stored at the tracking points.

1.1.3 Results from testing the model performance

The results for Tests 1, 2, 3 and 4 provided, for each fumarolic source, the Empirical Cumulative Density Functions (ECDFs) of the observed and simulated daily averages of H₂S and CO₂ concentrations. In particular, the ECDFs of the simulated concentrations are obtained either by randomly varying the gas fluxes (e.g., Allard et al., 2014; Tamburello et al., 2019). Being the investigation period of 13 days, to simulate daily variations in gas flux, we ran 11 simulations per day resulting in 143 total simulation runs, which implies a significant amount of computational time as one simulated day required nearly 3 h on a PC with a i5 dual-core processor. We also provided further numerical simulations by using a fixed flux at each fumarolic source as the most similar to the observed water vapour flux (1.10 kg s⁻¹ for G56, 0.93 kg s⁻¹ for TAS, and 1.63 kg s⁻¹ for CS, considering the estimates in Tamburello et al., 2019 and Jessop et al., 2021) for the entire period of simulation (13 days).

Test 1 and 2, similarly to ash dispersal models (e.g. Macedonio et al., 2016; Selva et al., 2018), seem to be indifferent to the selection of the reference input (local or regional) meteorological data: in fact, no remarkable differences were observed between Tests 1 and 2. This implies that either meteorological dataset could be used as input to the DWM. Also Test 3 showed that a low resolution DEM (25 m) does not affect the model outputs. On

the contrary, notable differences between the daily averages of observed and simulated concentrations are observed in Test 4 (**Fig. 4**), when the model accounted for a finer computational grid resolution (5 m).

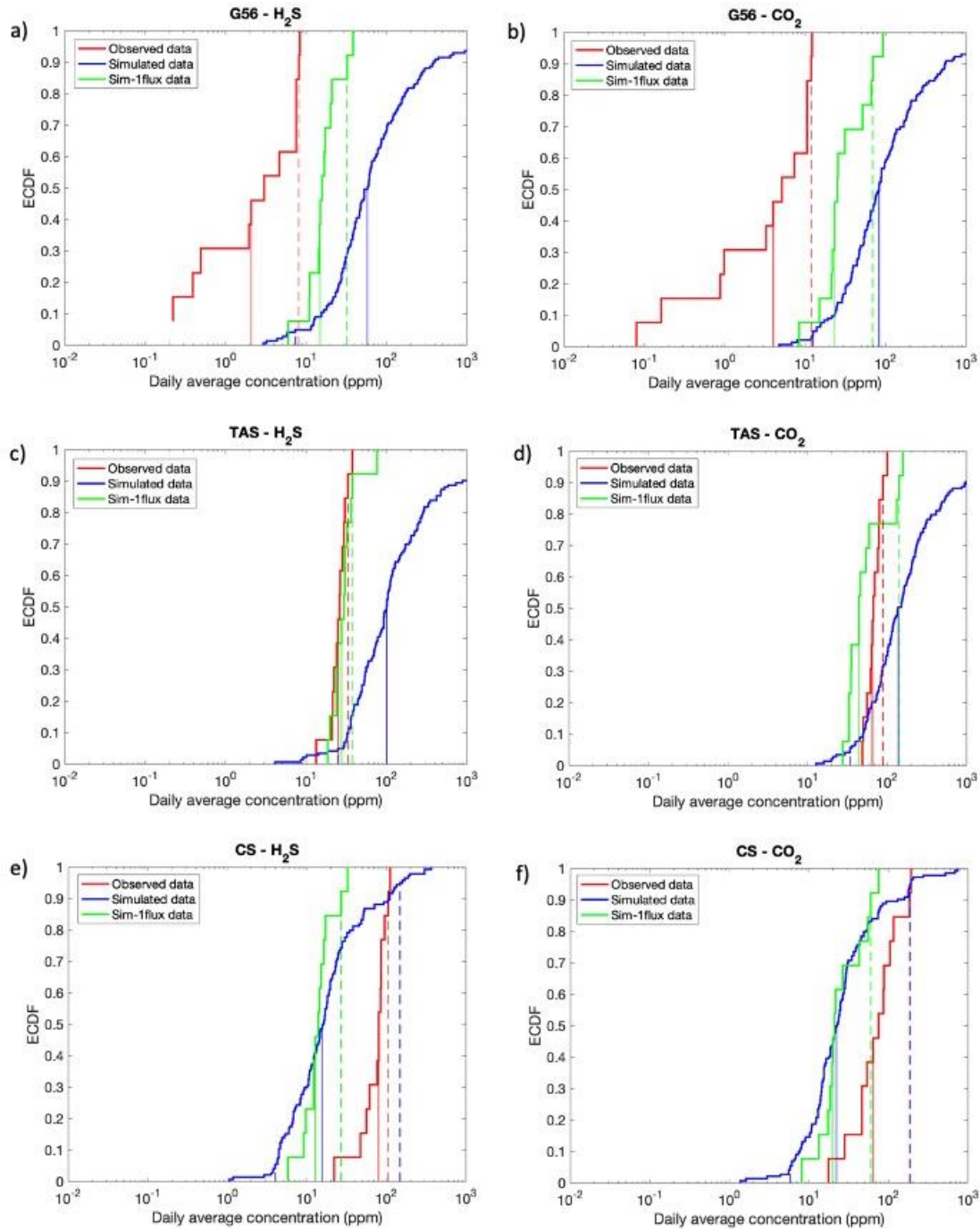


Fig. 4 - Results of Test 4 carried out with a computational grid resolution of 5 m. For each fumarolic source, the Empirical Cumulative Density Functions (ECDFs) of the observed and simulated daily averages of H_2S and CO_2 concentrations are shown for G56 (a-b), TAS (c-d), CS (e-f). The red curve represents the observed data while the blue and green curves refer to the simulated data obtained by randomly varying the water flux and by setting a fixed flux at source, respectively. The 50th percentile of the ECDFs is represented by the coloured vertical solid lines, while the 5th and 95th percentiles are represented by the dotted vertical lines. The topography is represented by a 5 m resolution DEM, from *Massaro et al. (2021)*.

In the following, for each single model output, we discussed some significant differences related to the three fumarole-station geometries at La Soufrière dome. First, Gouffre-56 fumarole is located in a deep fracture right below the eastern edge of the dome and is 3–4 m wide at the surface (**Fig. 3**). Its station has been forcibly located (as best compromise between proximity to the gas plume and sheltering from the strong winds) a few meters from the vent and windward with respect to the dominant wind. As a consequence, the observed data showed numerous cases of low volcanic gas concentrations, below the resolution of the sensor, that cannot be used for comparison with our simulations (see **Fig. 4a-b**).

Tarissan fumarole is a bubbling pond located in a ~ 40 m wide crater deep under the dome surface and its station is located ~8 m from the source and downwind with respect to the dominant wind. In this case, the fumarole-station geometry is the most favourable to provide the best accordance between model results and observations in each modelling setup (see **Fig. 4c-d**).

Cratère Sud is a system of three fumaroles located along a north-south oriented fracture in the southern edge of the dome. These fumaroles are ~10 m distant from each other and separated by spurs of rock. For the same logistic problems faced in G56, the station was installed in the southernmost part of the CS fracture, not exactly downwind of the degassing fumaroles. In this light, CS represents the most complex fumarole-station geometry.

In Tests 1–2–3 we noted that the underestimations of the simulated data with respect to the observations are balanced by using the 15 m- resolution grid (Massaro et al., 2021). When the simulations are carried out with the 5 m- resolution, the underestimations are more pronounced (see **Fig. 4e-f**) since the model algorithm tends to be numerically less diffusive by using a finer grid resolution.

On the whole, the model results showed an acceptable agreement with the observed data from a hazard point of view. This indicates the potential usefulness of gas dispersion modelling as a promising tool for reproducing the observed fumarolic degassing and for gas hazard assessment purposes.

1.2 Application of Great Balls of Fire model at La Soufrière de Guadeloupe to quantify hazard from volcanic ballistics

1.2.1 Introduction

In this study, we proposed a new probabilistic hazard quantification to provide the probability of Volcanic Ballistic Projectiles (VBPs) to exceed some critical kinetic energy thresholds, considering the variability of winds and eruptive vents, focusing on the most likely explosive scenarios at La Soufrière de Guadeloupe (including phreatic, Vulcanian and Strombolian eruptions) amongst those elaborated by the civil authorities in collaboration with the Observatoire Volcanologique et Sismologique de Guadeloupe (OVSG-IPGP) and listed in the emergency plan for volcanic phenomena that was adopted by the Préfet de Guadeloupe (Dispositions Spécifiques ORSEC de La Guadeloupe: phénomènes volcaniques, 2018,

<https://www.guadeloupe.gouv.fr/content/download/15808/103240/file/Dispositions%20sp%C3%A9cifiques%20ORSEC%20de%20la%20Guadeloupe%20-%20Ph%C3%A9nom%C3%A8nes%20volcaniques.pdf>).

The definition of a probability distribution of the impact energy or impact size represents the base for the hazard quantification adopted in this work: the hazard associated with the adopted eruptive scenario is quantified by the probability of exceeding a given energy (or clast size) threshold defined, which in turn is derived from the energy (or size) distribution in each given cell as probability of exceeding the threshold. Therefore, at the end of the process each cell is described in terms of an “exceeding probability referred to a hazardous threshold”.

Here we quantified the probability of ballistic impact to exceed energy thresholds for roof perforation (E_t , minimum impact energies to penetrate some reference materials; Spence et al., 2008; Williams et al., 2017) considering the most frequent roof types in Guadeloupe.

The results of this study are included into a paper (Massaro, S., Rossi, E., Sandri, L., Bonadonna, C., Selva, J., Moretti, R., Komorowski, J.-C. “Assessing hazard and impact associated with volcanic ballistic impacts: the example of La Soufrière de Guadeloupe volcano, Lesser Antilles”), which is currently submitted to Journal of Volcanology and Geothermal Research.

1.2.2 Methodology

In this study, the simulated VBP locations were obtained from a forward use of the Great Balls of Fire model (Biass et al., 2016) and validated by means of observed data from La Soufrière (Komorowski, 2015).

The procedure implemented to assess quantitatively the probabilistic hazard is based on the independent evaluation of the probability of exceeding a given energy threshold and the probability of having clast fallout of a given size per cell. This results in an alternative version of the post-processing routine which has been specifically coded in MATLAB (available at

https://github.com/silfromitaly1/probabilistic_hazard_assessment_for_ballistics).

We defined the exploration of the potential vents only considering the spatial probability of vent opening within the dome area due to the limited computational resources provided by our calculators.

In **Figure 5** (a-b) we show the spatial probability of vent opening map built following the approach by Selva et al. (2012) and based on existing literature data on the main geological structures, historical eruptive vents, past observed fumarolic activity and measurements of the present-day gas emission rates. To reach a balance between computational feasibility and accuracy, we focused on the dome area which is the most likely zone for phreatic events in the future, due to past eruptive vent locations and the on-going degassing activity. Thereafter, we identified four macroareas covering the dome (A1, A2, A3, A4; **Fig. 5c**).

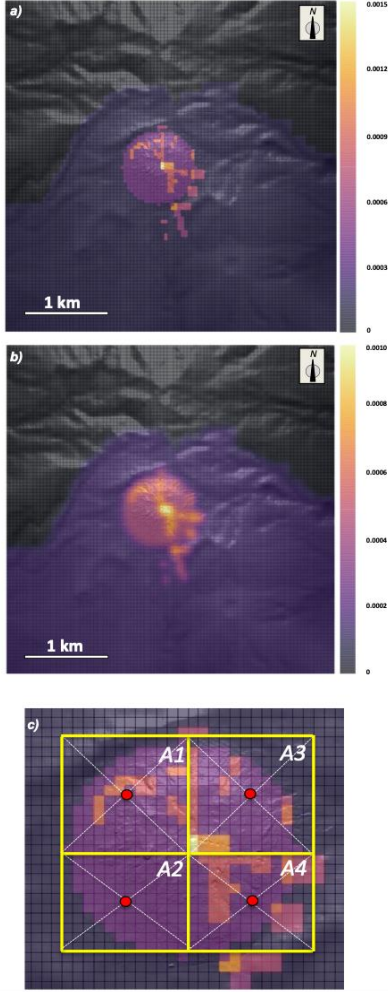


Fig. 5 - a) Best-guess probability map of vent opening; b) Gaussian filter with $\sigma = 40$ m applied to consider the spatial uncertainty of the data and to avoid a scattered spatial distribution due to the limited sampling; c) Magnification of the spatial map displaying the probability of vent opening within four regular macroareas (A1, A2, A3, A4). The corresponding vents are located in the centre of each macroarea (red dots), from **Massaro et al., submitted**.

After having carried out a sensitivity analysis on the number of simulated VBPs, we run GBF launching $2 \cdot 10^6$ VBPs from the centres of the four macroareas on the dome (**Fig. 5c**), assuming that these simulations can be representative of the whole macroarea.

Under these assumptions and considering the total probability theorem, we computed the overall probability, conditional on the selected scenario, for roof perforation in a given area when a VBP is ejected. This probability is quantified as the product of the conditional probability to exceed a given threshold ($E_t = 360$ J, timber weatherboard, $E_t = 650$ J, sheet material, and $E_t = 2750$ J, reinforced concrete) when a VBP falls in the cell (i.e.,) and the probability that a clast reaches that cell, In formulas:

$$\theta^f_{A_{ij}} = \sum_{k=1}^{k=4} \omega'_k \left[\theta^f_{A_{ij,k}} \right] = \sum_{k=1}^{k=4} \omega'_k \left[\frac{n_{VBP,A_{ij,k}}}{n_{VBP}} \right] \quad (1)$$

$$\theta^{ec}_{A_{ij,m}} = \sum_{k=1}^{k=4} \omega'_k \left[\theta^{ec}_{A_{ij,E_{tm,k}}} \right] \quad (2)$$

$$\theta^e_{A_{ij,m}} = \sum_k \omega'_k \theta^e_{A_{ij,E_{tm},k}} = \sum_k \omega'_k [\theta^{ec}_{A_{ij,E_{tm},k}} * \theta^f_{A_{ij,k}}] \quad (3)$$

where ω'_k represents the vent opening probability associated to each macroarea which is the sum of the probabilities of vent opening of the cells of the finer vent-grid belonging to that macroarea (**Fig. 5c**).

1.2.3 Sensitivity analyses

In order to assess the effect of the wind on simulation results, we calculated the relative difference in the conditional exceedance probability to overcome the selected energy thresholds obtained by comparing results with minimum wind conditions (taken by the “Piton Sanner” meteorological station during 2017-2018) and in absence of wind (**Fig. 6a**). The differences are less than 5% for and reach values up to 15% for in few cells, showing unstable relative differences (incoherent pattern for adjacent cells) at greater distances. Very similar results are obtained considering the maximum and absent wind conditions; **Fig. 6b**). Considering this, we conclude that wind does not significantly affect the probability results within a few km from the vent.

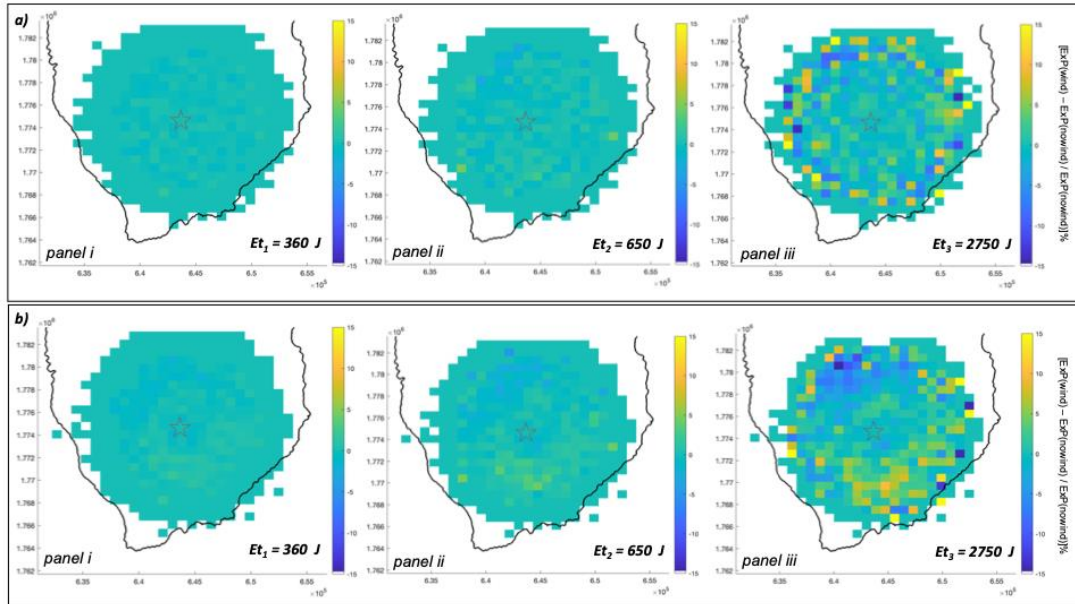


Fig. – Sensitivity analysis on wind conditions showing the relative difference between the exceedance probabilities referred to $E_t = 360$ J (panel i), $E_t = 650$ J (panel ii), and $E_t = 2750$ J (panel iii), in case of a) minimum ($W_s = 2$ m s⁻¹, $W_d = 279^\circ$) and absent wind conditions. The same test was carried out in considering b) maximum ($W_s = 25$ m s⁻¹; $W_d = 343^\circ$) and absent wind conditions. For all tests, the vent is located at the centre of the dome area (star), from *Massaro et al., submitted*.

We also provided the sensitivity analysis to the position of the vent on the computational domain. In **Figure 7** we show the comparison between the conditional exceedance probabilities for $E_t = 2750$ J) derived from i) assuming one hypothetical scenario of a single vent (for which we assume to be certain about position on the dome), and ii) considering the uncertainty on vent position, combining more vents. Remarkable differences are observed when simulations account for a single vent as a hypothetical scenario (**Fig. 7a-b**) and for the uncertainty on vent opening from the dome area (**Fig. 7c**). In the latter case, we show that the uncertainty on the vent position “blurs” the resulting hazard or probability maps (e.g., Sandri et al., 2016); however, it represents more “honestly” our degree of knowledge on future eruptions (for which we actually do not know the effective vent position), leading to spatially unbiased probability maps.

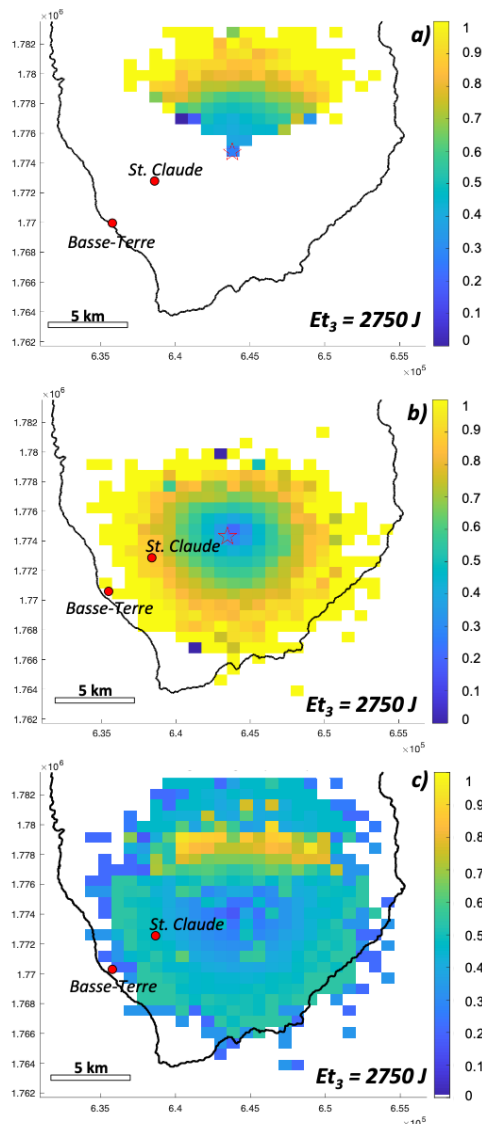


Fig. 7 - Probability maps to exceed (2750 J) considering the hypothetical scenario of a single vent located at a) 643820 E; 1774748 N, and b) 643451 E; 1774316 N; c) Probability map to exceed (2750 J) considering the uncertainty on vent opening through the combination of more vents on the dome area, from **Massaro et al., submitted**.

The sensitivity analysis to the position of the vent highlighted how the spatial variability of vents opening is pivotal in this hazard assessment study since the resulting impact could affect the surrounding community at multiple scales in case of the adopted scenario.

1.2.4 Hazard results and analysis of the potential impacts

The probability maps derived from equations (1-2-3) provided an opportunity to identify the main urban areas likely to be impacted at La Soufrière in case of an eruption of the adopted scenario from the dome area. In this study, we combined the exposed elements (i.e., schools, hospitals and clinics, towns, villages, and the airport) with the probability results obtained with equations (1-2-3), in absence of wind.

Hazard and exposure aspects have been combined to produce an exposure-based risk map shown in **Figure 8**. Considering the conditional probability (eq. 2), results showed that a large portion of the Basse-Terre town would be affected by the VBP impacts that exceed the energy thresholds for roof perforation with a probability in the range of 20-60%, with the exception of a limited sector showing a higher probability (>80%) (**Fig. 8**, panels a-b-c). On the contrary, when the overall probability is accounted for, the probability is exclusively restricted to a few kilometres from the dome area and shows lower values to overcome the selected energy thresholds (from ca. 2%

up to 40%) (Fig. 8, panels d-e-f). This means that in areas where urban agglomerates are within a few km from the vent such as the case at La Soufrière, the choice of a probabilistic approach is key to estimate the likelihood of occurrence of VBPs impacts as a first step towards the development and implementation of pro-active risk reduction strategies.

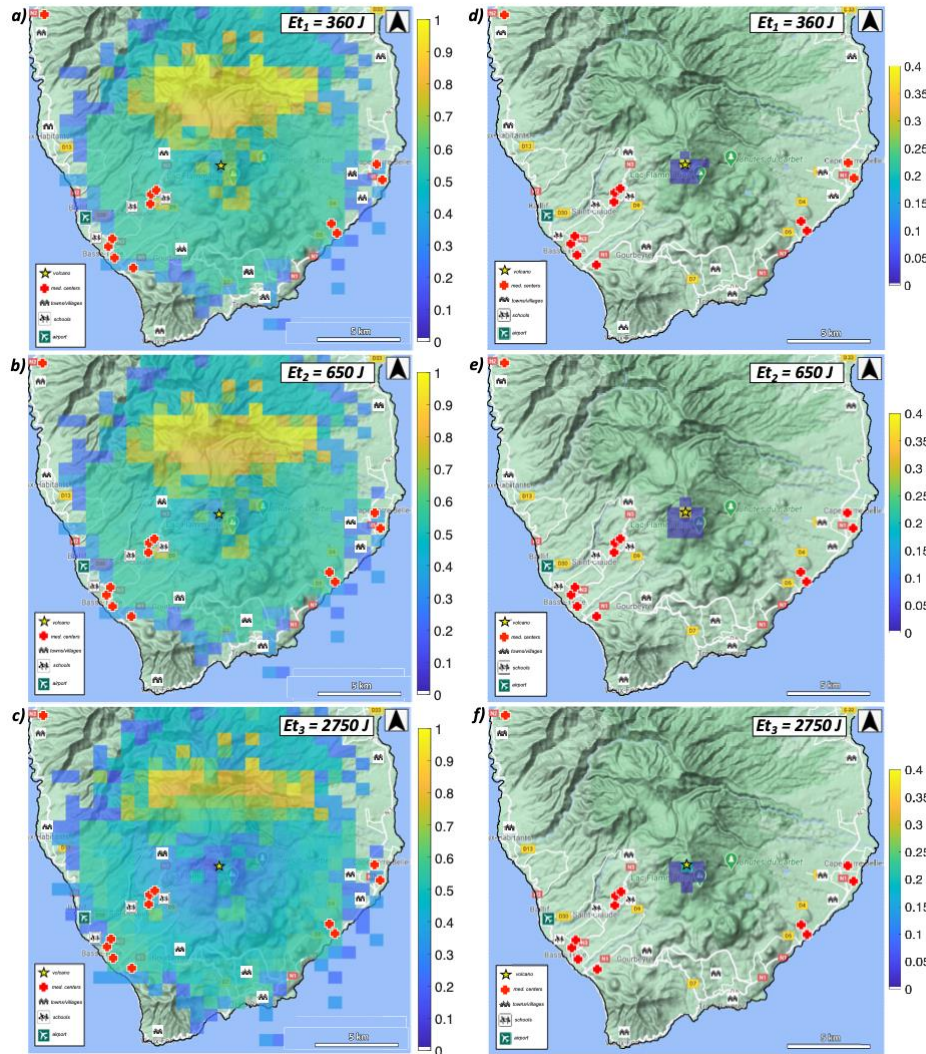


Fig. 8 - Exposure-based risk analysis considering the conditional probability (a-b-c) and the overall probability (d-e-f) of VBPs exceeding selected energy thresholds. All probabilities are conditional to the ejection of a clast during an eruption within the adopted scenario and from the dome, in absence of wind. Symbols in legend: yellow star: La Soufrière volcano; red cross: hospitals and clinics; two-houses: towns (i.e., St. Claude, Basse-Terre) and villages (i.e., Matouba and Papaye); running children: schools; airplane: airport), from **Massaro et al., submitted**.

1.3 Application of the PDAC model at La Soufrière de Guadeloupe to quantify hazards from pyroclastic currents resulting from the collapse of explosive Sub-Plinian and Plinian eruption columns, case study of the 1530 C.E. eruption at La Soufrière de Guadeloupe

(published in Esposti Ongaro et al., 2020; see cover page in Figure A2)

1.3.1 Introduction

La Soufrière de Guadeloupe is an andesitic composite volcano whose activity over the last 10,000 years has been characterized by a diversity of eruptive styles, including effusive and dome-forming eruptions, explosive phreatic or hydrothermal and magmatic (Vulcanian to plinian) eruptions, and numerous flank collapse events (Komorowski et al. 2005; Boudon et al. 2007; Legendre 2012; Peruzzetto et al., 2019). The most recent magmatic subplinian eruption dates from 1530 CE (Boudon et al. 2008; Komorowski et al. 2008), and a smaller magmatic (Vulcanian to subplinian) eruption took place in 1657 CE (Legendre 2012; Rosas-Carbajal et al. 2016). The historical activity since the 1657 eruption has been characterized by minor (1690, 1812, and 1956) and major (1797–1798, 1836–1837, and 1976–1977) non-magmatic (phreatic) eruptions. These eruptions have taken place from fractures and vents on La Soufrière de Guadeloupe's lava dome (Feuillard et al. 1983; Komorowski et al. 2005; Rosas-Carbajal et al. 2016). The last and most violent phreatic eruption occurred in 1976–1977 and forced the evacuation of about 73,600 people for up to 4 months. Although it did not evolve into a magmatic eruption, geophysical and geochemical evidence supported its interpretation as a shallow intrusion that did not feed an eruption (Feuillard et al. 1983; Villemant et al. 2014). This failed magmatic eruption (Moran et al. 2011) involved a small-volume magma intrusion that ascended from the 6–8.5-km-deep magma reservoir (Pichavant et al. 2018) and stagnated at shallower depth, pressurizing the hydrothermal system at a depth of about 500 m below the summit (Feuillard et al. 1983; Komorowski et al. 2005; Villemant et al. 2014; Hincks et al. 2014).

Although interpretation of the eruptive history of La Soufrière de Guadeloupe has been particularly difficult on account of erosion and alteration processes that are particularly intense under the tropical climate, geological studies suggest there have been several magmatic explosive eruptions in the last 10,000 years including at least two subplinian VEI 2–3 and six Plinian VEI 4 (Komorowski et al. 2005; Legendre 2012). The 1530 CE eruption is representative of a typical subplinian (VEI 3) magmatic explosive eruption at La Soufrière de Guadeloupe and is interpreted to be the most credible eruptive scenario for a future event (Boudon et al. 2008; Komorowski et al. 2008; Spence et al., 2008).

Seismic, fumarolic, and thermal unrest at La Soufrière de Guadeloupe has been slowly increasing since 1992 (Komorowski et al. 2005; OVSG-IPGP 1999–2020). In April 2018, the unrest reached its highest level since the end of the 1976–1977 failed magmatic eruption (Moretti et al. 2020; OVSG-IPGP 1999–2020). Although the alert level has remained at yellow (vigilance), the increasing unrest has prompted reinforced monitoring by the Volcanological and Seismological Observatory of Guadeloupe (OVSG-IPGP) and the decision by authorities to implement an exclusion zone for the general public to the most active areas of the summit (Préfet de la Région Guadeloupe, 2019).

1.3.2 Methods

Following Komorowski et al. (2008) and Boudon et al. (2008), the last magmatic eruption of La Soufrière de Guadeloupe in 1530 CE is taken as a reference scenario for assessing hazards associated with PDC emplacement. For the 1530 CE eruption, the column height has been estimated at between 9 and 12 km from tephra fall deposits by Komorowski et al. (2008). This corresponds to an estimated peak mass eruption rate of between 5.5×10^6 and 1.3×10^7 kg/s, i.e. in the range of subplinian eruptions. With new field data (Legendre 2012), the column height has been determined to have reached 16 to 18 km, for a mass eruption rate on the order of 7×10^6 – 2×10^7 kg/s, a volumetric flux of 4 – 7×10^3 m³/s, and an estimated minimal eruption duration of 0.7 h (Komorowski et al. 2013) with realistic eruption conditions (volatile content between 2 and 5 wt.% and temperatures between 950 and 1100 °C) that characterize a threshold between a convective and collapsing plume regime, which can be termed a transitional or oscillating regime. To reconstruct the mass eruption rate at the time of collapse during transitional regimes, we have assumed, based on Wilson et al. (1980), that this is equal to the maximum intensity achieved during the convective phase. Numerical investigations of Trolese et al. (2019) demonstrate that plume height is strongly reduced during partial collapse episodes, so that the mass eruption rate might be underestimated. Moreover, full collapse of a subplinian column can be triggered by the downward collapse of the edifice into an emptying chamber to form a summit caldera. Although there is no clear evidence for a summit caldera collapse at La Soufrière de Guadeloupe during the 1530 CE eruption, a sudden enlargement of the vent might have resulted

as a consequence of an initial phase of partial lateral flank collapse. Moreover, geophysical imaging (i.e. electric conductivity, Rosas-Carbajal et al. 2016) indicate the presence of an arcuate vertical structure to the South-West and South of the current dome that may mark the relict margins of the explosion crater associated with the eruption within which the dome grew at the end of the eruption (Boudon et al. 2008). Overall, the structural features surrounding the current dome show a combination of an explosion crater and edifice collapse structure that is roughly circular and about 900 m in diameter. Therefore, we also considered a scenario with an enlarged vent diameter.

Here, we use the three-dimensional, multiphase flow model PDAC (i.e. Pyroclastic Dispersal Analysis Code; Neri et al. 2003; Esposti Ongaro et al. 2007; Carcano et al. 2013) to numerically simulate the development, instability, and collapse of a subplinian eruption column and the generation and propagation of PDCs over the topography around La Soufrière de Guadeloupe. All model equations and the main underlying assumptions are summarized in Appendix 1 of Esposti Ongaro, et al. (2020). The advantage of using non-equilibrium multiphase flow models is that they offer a comprehensive description of stratified PDCs (see Esposti Ongaro et al. 2020 and references therein). In particular, 3D models can describe PDC proximal stratification, formation of the basal layer by particle settling, and generation of an overlying ash cloud due to shear flow mechanisms. The reliability of the PDAC model in describing the main large-scale behaviour of volcanic plumes, for the range of mass eruption rates apparent here, has been demonstrated by a 3D plume model inter-comparison study (Costa et al. 2016; Suzuki et al. 2016; Esposti Ongaro and Cerminara 2016). We base our discussion of model-related uncertainty on the relatively large number of 3D numerical simulations performed in this study (Esposti Ongaro et al., 2020), with input conditions derived from field work carried out at La Soufrière de Guadeloupe and published in Boudon et al. (2008), Komorowski et al. (2008, 2012, 2013), and Legendre (2012). In evaluating the reliability of our results and the potential effect of the adopted numerical approximations on the model output, we also rely on published 2D/3D numerical simulations by Esposti Ongaro and collaborators made at Vesuvius, Soufrière Hills, Montserrat, Campi Flegrei, Mount St. Helens, as well as similar modelling studies by other authors (see Esposti Ongaro et al., 2020 for references).

Our modelling assumes a sustained event, i.e. stationary conditions at the vent producing a collapsing column. Steady-state boundary conditions are imposed at the vent, coinciding with the exit section of the crater. We initially assume an average mass flow rate of $7 \times 10^6 \text{ kg s}^{-1}$ ejected from a circular vent located on the present summit of the La Soufrière de Guadeloupe dome, as based on Komorowski et al. (2008). Initial temperature was set to 1050 K (777 °C) and water content to 2 wt.%, resulting in a mixture density of around 12 kg/m^3 . The granulometry of juvenile particles was derived from data given in Komorowski et al. (2008) by adopting three particle classes with diameters of 1000 μm (50 wt.%), 250 μm (24 wt.%), and 30 μm (26 wt.%), and densities of 1200, 2000, and 2,600 kg/m^3 , respectively. Although this granulometry is finer than the actual subaerial deposit of the 1530 CE eruption of La Soufrière de Guadeloupe, it represents a compromise between the need to account for a relatively coarse component of the pyroclastic phase and the capability of our numerical model to treat coarse-grained phases. The three particulate phases are initially in mechanical and thermal equilibrium with the gas, but they are characterized by different degrees of coupling with the carrier fluid flow, so that non-equilibrium phenomena (between gas and particles and between different particles) developing during the eruption can be analysed with the model. Details of the input parameters are found in Esposti Ongaro et al. (2020).

Four scenarios have been selected, named SP1 through SP4, whose main input parameters are given in Tables 1 and 2.

Table 1 - Properties and mass/volume fractions of solid particle phases (named P1, P2, and P3) used to represent the input grain size distribution for numerical simulations SP1–SP4 in Table 2. Grain size data are taken from Komorowski et al. (2008). Taken from *Esposti Ongaro et al., 2020*

Phase	Gas	P1	P2	P3
Diameter [μm]	n.a.	1000	200	50
Density [kg/m^3]	0.21	1200	2000	2600
Bulk density [kg/m^3]	0.21	6.0	3.0	3.12
Mass fraction [wt. %]	1.7	48.7	24.3	25.3
Relative solid mass fraction	n.a.	49.5	24.8	25.7
Volume fraction	0.9923	0.0050	0.0015	0.0012

Table 2 - Input parameters for the four simulated scenarios of Subplinian eruption collapse at La Soufrière of Guadeloupe. Taken from *Esposti Ongaro et al., 2020*.

	SP1	SP2	SP3	SP4
Input				
Inlet radius [m]	38	45	52	104
Inlet velocity [m/s]	127	90	70	70
Gas pressure [Pa]	10^5	10^5	10^5	10^5
Mixture density [kg/m^3]	12	12	12	12
Mixture temperature [K]	1050	1050	1050	1050
Water content [wt. %]	2	2	2	2
Mass flow rate [kg/s]	7×10^6	7×10^6	7×10^6	2.8×10^7
Output				
Estimated percentage of collapse ($\pm 10\%$)	50%	70%	90%	90%

1.3.3 Results

Numerical simulations describe in 3D the formation of the volcanic jet, its instability and partial collapse, resulting in the simultaneous formation of a sustained plume and PDCs. Scenarios SP1 and SP2 are partial collapse scenarios while scenarios SP3 and SP4 are full collapse scenarios. **Fig. 8** shows the results for the full collapse scenario SP4 at different times during the simulation. Further details on the results are in a published paper by Esposti Ongaro et al. (2020) (See the appendix for a picture of the front cover **Figure A.2**).

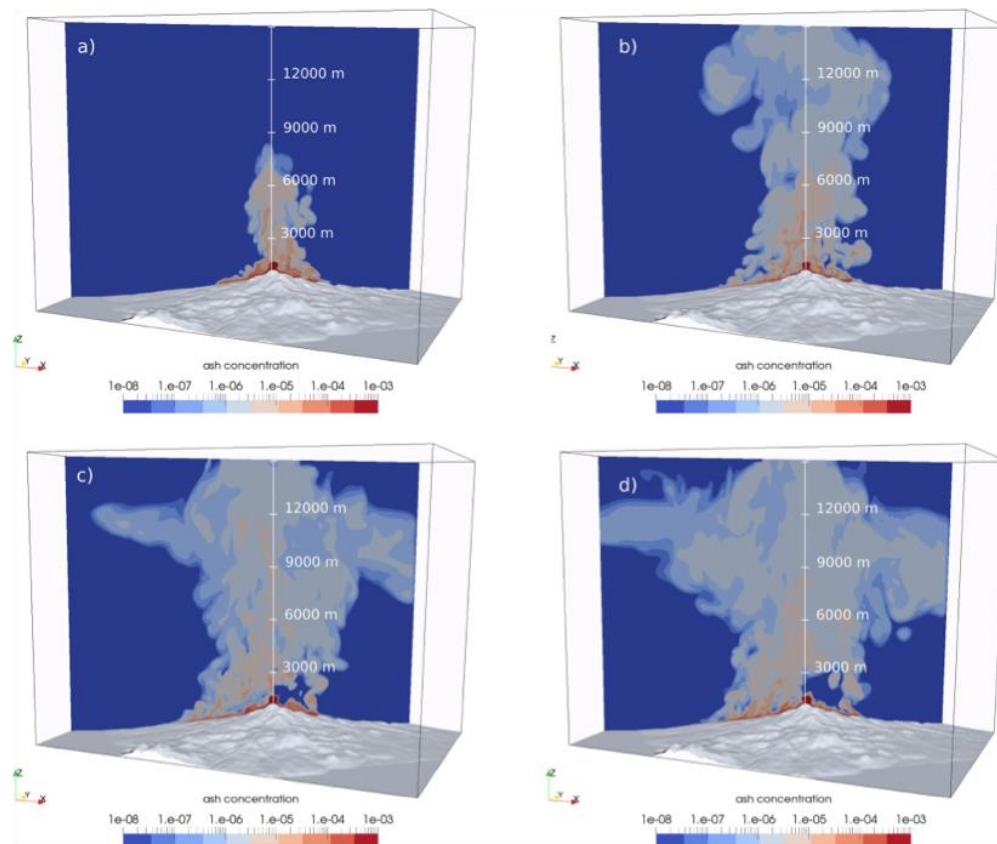


Fig. 8. 3D sequence of full (> 90%) collapse, with increased mass eruption rate of about 3×10^7 kg/s (run SP4) at $t = 200$ s, $t = 400$ s, $t = 600$ s, and $t = 800$ s after the beginning of the collapse phase. The colour scale represents the volume concentration of the fine ash (diameter $50 \mu\text{m}$) on a logarithmic scale (Taken from *Esposti Ongaro et al., 2020*).

Maps of PDC invasion were plotted by interpolating the 3D numerical results on isosurfaces at constant height above the topography. We take the first cell above the topography as representative of ground-level PDC conditions. Ground-level values are thus average values for the first 20 m above the topography (10 m for fine mesh simulations; Appendix 1, Esposti Ongaro et al., 2020). Such averaging is implicit in the adopted finite volume computational technique and numerical grid. We use temperature and dynamic pressure (i.e. the kinetic energy per unit of volume) as the two most significant variables for hazard assessment (Esposti Ongaro et al. 2002; Gurioli et al. 2005) (see Esposti Ongaro et al, 2020 for details). Maps of temperature (**Fig. 9**) are shown at the final simulation step (i.e. after 300 s for SP1, 380 s for SP2, 550 s for SP3, and 800 s for SP4). This is the time at which the most concentrated (basal) part of the current stops to advance. Following past simulation experiments and comparisons with real PDC events (e.g. Esposti Ongaro et al. 2008b, 2012) suggests that this is the best estimate of the actual PDC runout, even though the dilute cloud is still capable of slow advance, especially in the absence of wind and atmospheric turbulence in the model description. For dynamic pressure (**Fig. 10**), we plot the maximum value reached at each grid point during the simulation. As a reference, a dynamic pressure of 1 kPa is sufficient to break windows, whereas at 10 kPa failure of reinforced masonry can be expected (Jenkins et al. 2010, 2013a).

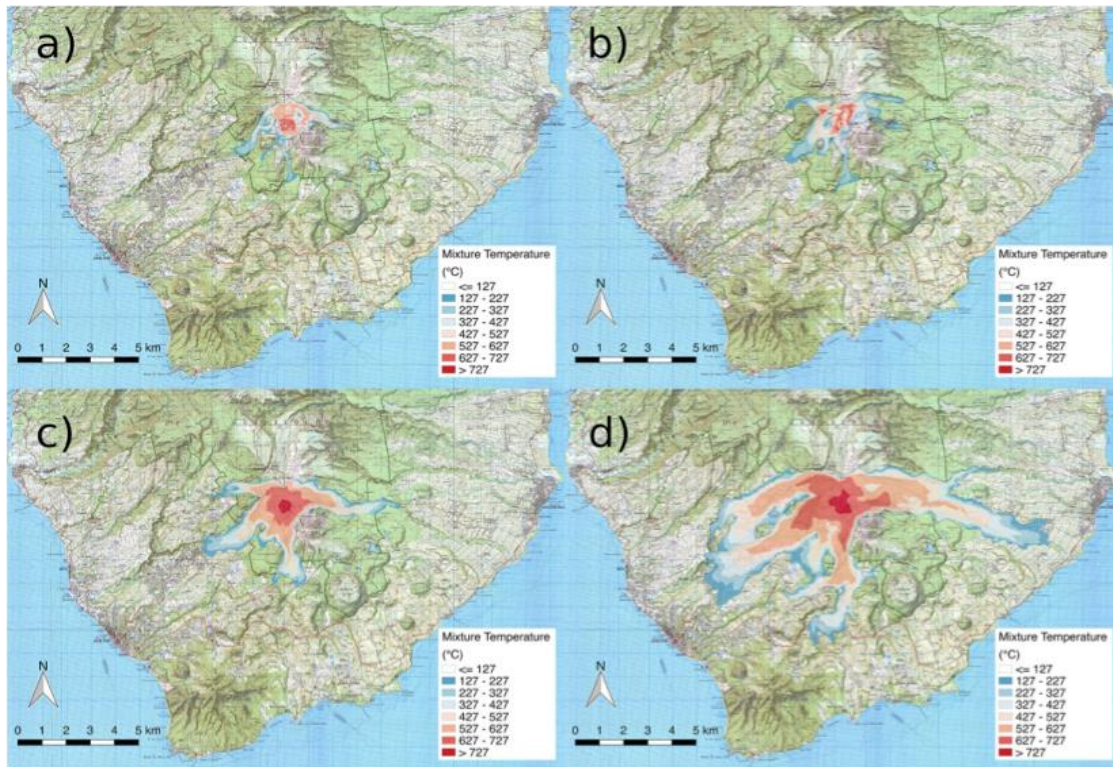


Fig. 9. Final maps of mixture temperature superposed to the IGN cartography, showing the inhabited regions around the volcano. Maps are given for simulations a SP1, b SP2, c SP3, and d SP4 (Taken from Esposti Ongaro et al., 2020).

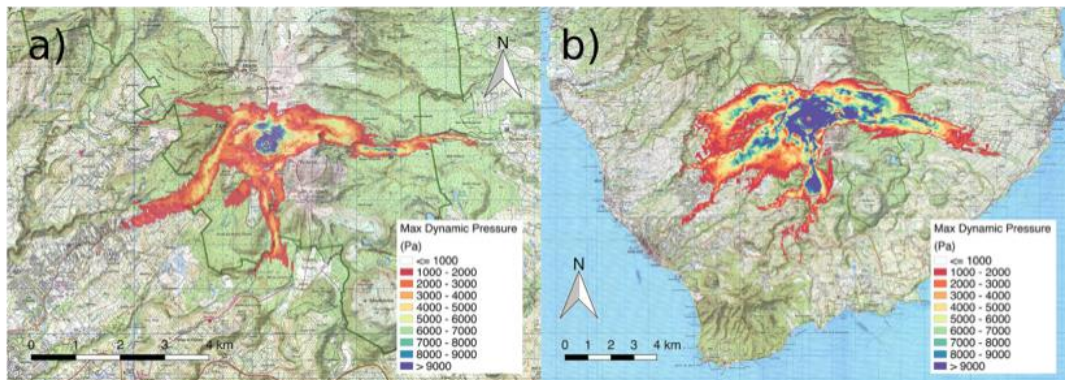


Fig. 10. Maps of maximum dynamic pressure estimated for each point in the domain for scenarios a SP3 and b SP4 (Taken from Esposti Ongaro et al., 2020).

Drawing hazard maps for a single scenario, based on numerical model results, is still a challenging task that cannot be performed in a fully automatic way. It needs, instead, some expert judgement to account for model uncertainties (Calder et al. 2015). In particular, we have to consider the uncertainty associated with numerical errors and incomplete physical description of the phenomenon. Here, we have used different isolines of temperature to identify the areas reached by the most concentrated, basal part of the current and by the dilute ash cloud. In Fig. 10, we propose a preliminary identification of two hazard regions based on temperature isolines for both simulations SP3 and SP4. The 600 K isoline (327 °C) is considered as the region very likely invaded and highly impacted by PDCs, for the selected scenario. This is based on the following considerations:

- The isoline is stable and stationary in time (it does not further advance, once it reaches the displayed limit)
- This temperature threshold almost coincides with the limit of significant dynamic pressures (i.e. > 1 kPa) and of the maximum distance reached by the more concentrated (particle volume concentration of $> 10^{-3}$) basal layer
- Its position corresponds quite well with the limit of satisfactory vertical discretization (> 5 cells in the boundary layer) of the stratified PDC

The 300 K (27 °C) isoline, on the other hand, encloses an area susceptible to PDC invasion and moderately impacted. In this area, simulated PDCs are mostly dilute, have temperatures of between 27 and 327 °C (still capable of causing severe injuries; Baxter et al. 2005, 2017), and have dynamic pressures of lower than 1 kPa. Here, however, the numerical uncertainty on the prediction is much larger and is more influenced by the physical approximations of the model (mostly, incomplete description) and by approximate boundary conditions at the ground surface. Finally, the area outside of the 300 K (27 °C) isoline should be considered as unlikely to be invaded or marginally impacted by PDCs in the selected scenario, mostly because it is sheltered by significant topographic barriers or because of the great distance between the source and the location. However, it is important to note that different vent location, geometry, and eruption conditions, as well as atmospheric conditions, could potentially change the results for such a deterministic scenario. Therefore, the zonation presented here should be considered as a preliminary product to be refined in the future.

The use of clear and quantitative hazard maps for an individual scenario, in combination with three-dimensional visualization techniques (Fig. 11), can provide the tools for a better evaluation and communication of the hazards associated with a future scenario of a subplinian eruption at La Soufrière de Guadeloupe, and contribute to a more effective risk management strategy. To aid with this, our Electronic Supplementary Material (Esposti Ongaro et al., 2020) presents video animations for the development of a subplinian column and PDCs in scenario SP4, looking from the South-West (PDC branch moving towards the town of St Claude; Online Resource 1, Esposti Ongaro et al., 2020) and looking from the South (PDC branch moving towards the town of Capesterre; Online Resource 2, Esposti Ongaro et al., 2020).

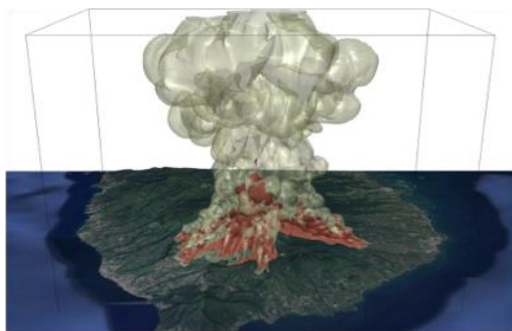


Fig. 11. Example of visualization of 3D results for communication purposes. Simulation SP4 of total ($> 90\%$) collapse, with increased mass eruption rate of about 2.8×10^7 kg/s (run SP4), 400 s after the beginning of the collapse phase. Isosurfaces of 10^{-7} (outer, light green) and 10^{-5} (inner, brown) for the volume concentration of the fine ash are superimposed on a DEM of the volcano draped with satellite images (Google ©2018 Maxar Technology). Taken from Esposti Ongaro et al., 2020.

1.3.4 Conclusions

We have presented the results of a numerical study aimed at assessing the factors controlling propagation, emplacement, and hazards of PDCs in a credible (cf. Baxter et al. 2008) subplinian eruption scenario at La Soufrière de Guadeloupe. A set of deterministic simulations were constrained using the best estimates of eruption source parameters. One of the outcomes is that, even with a narrow range of mass eruption rates, subplinian eruptions can display very different eruptive styles, with different impacts from associated PDCs. Although exploration of a more extended range of eruptive conditions and a systematic appraisal of uncertainties would be necessary to perform a complete hazard assessment study, present results allow us to draw some preliminary conclusions and to contribute to the assessment of hazard associated with a potential future reawakening of the volcano.

Low-intensity (7×10^6 kg/s) subplinian plumes are able to generate an oscillating column and steeply stratified PDC by a mechanism of partial collapse (50 to 70% of mass collapsing). Despite their ability to surmount proximal topographic barriers, PDC runout would be limited to the first 2–3 km from the vent and impacts on the inhabited region would be negligible. It is however possible (but not addressed by our modelling) that such weak plumes could be influenced by strong winds or asymmetric vent conditions, enhancing PDC runout in certain sectors.

Although partial collapse episodes are on average isotropic, the distribution of PDCs is asymmetric, due to the strong topographic control at the horseshoe-shaped collapse structure in the summit area. All simulations show that, given the present morphology of the La Soufrière de Guadeloupe volcano, most of the PDC mass will be focussed to the East-Northeast (which will take between 25 and 30% of the total mass), West-Southwest (between 25 and 50%), and South (10 and 15%), with a smaller portion (less than 5%) being emplaced in the North-Northwest sector. Between 5 and 30% will remain within the limits of the summit area.

Fully collapsing (fountaining or boiling over) conditions (90% of collapse) can be generated by a sudden enlargement of the vent (e.g. by a syn-eruptive partial edifice collapse such as that which occurred in the 1530 CE eruption, Boudon et al., 2008), with a consequent reduction of the average exit velocity (at the same mass eruption rate) and air entrainment. In such a case, PDC intensity (mass flow rate per unit of angle), mobility (including capacity of surmounting topographic barriers), and the consequent impact on surrounding populations can be strongly enhanced, potentially affecting the inhabited regions > 4 km from the vent.

Increase in the mass flow rate at the vent to about 2.8×10^7 kg/s (or funnelling of the collapsing mass into a single sector) is sufficient to generate more mobile PDCs that are able to reach the inhabited regions about 6 km from the vent. This is particularly the case as PDC mass is focussed in deep valleys and canyons (> 100 m deep) that reach far into the inhabited areas. Pyroclastic density currents with dynamic pressures exceeding 3 kPa and temperatures exceeding 200 °C can be expected in such cases and this is sufficient to inflict considerable damage to buildings and will be lethal to humans and animals (Baxter et al. 2005). Following Jenkins et al. (2013a), we will thus use, in a future study, the resulting spatial distribution of peak temperatures and dynamic pressures to develop a quantitative impact model for the population, infrastructure, and communication/facility networks. This will be combined with vulnerability information derived from medical analyses (cf. Baxter et al. 2017) and building engineering (cf. Jenkins et al. 2013b), and with exposure data, to quantify the risk.

Finally, by combining information on the spatial distribution of temperature and dynamic pressure with objective considerations regarding model-related uncertainty, we are able to draw preliminary PDC hazard maps for a subplinian eruptive scenario. This still requires some level of expert judgement to identify the factors that control uncertainty of numerical simulation results. In such a representation, and for the reference subplinian scenario, we identify three areas varying in susceptibility to invasion by PDC: very likely to be invaded (with dynamic pressures of > 1–10 kPa and temperatures of > 300 °C), susceptible to invasion (with lower dynamic pressures and temperatures), and unlikely to be invaded by PDCs. This information will need to be updated in the future by considering a broader set of eruptive conditions and uncertainties. However, we believe that, given the current increasing unrest, it can provide a useful and timely contribution to hazard assessment and crisis response in the advent of a future eruption at La Soufrière de Guadeloupe, while being a blueprint as to how to set-up hazard maps for subplinian eruption scenarios elsewhere.

This work thus contributes to a volcanic risk assessment strategy in Guadeloupe initiated several years ago (Komorowski et al. 2005, 2008, 2013; Hincks et al. 2014; Legendre 2012; Peruzzetto et al. 2019; Leone et al. 2019), with the first integrated hazard map for La Soufrière de Guadeloupe being produced by Komorowski et al. (2005). Subsequently a first attempt to characterize the eruptive behaviour in a systematic way was carried out by Komorowski et al. (2008), who defined a logical event tree for magmatic unrest and eruptions. Using this framework, and by means of a combined field study and numerical simulations, Komorowski et al. (2008) analysed the hazards associated with the tephra fallout phase in a subplinian scenario similar to the 1530 CE event. Considering the recurrence of PDCs in the volcanic history of La Soufrière de Guadeloupe, and the evidence of PDC deposits in urbanized areas (Legendre 2012), it seems very likely that for such a future magmatic eruption, PDCs could affect, directly or indirectly, a very large part of the South of the island of Basse-Terre, where some 70,000 people live. Given the topography of the area and the geometry of rivers that drain the volcano and reach the inhabited areas, one of the most important issues of the hazard and impact assessment is to model the influence of the topography on the mobility and dynamics of the PDCs and the associated inundation areas.

2 – Application of previously existing hazard and risk tools to other volcanoes

2.1 Application of HASSET tool to San Miguel, Salvador

2.1.1 Introduction and context

From the 23 volcanoes in El Salvador, at least 5, are known to be currently active. Despite all five active centers being located very close to inhabited areas and a large amount of infrastructures, volcanic hazard assessment studies in the country are scarce. San Miguel is one of the most active volcanoes of El Salvador with, at least, 28 eruptions in the past 430 years. The volcano is surrounded by several villages and cantons, which could be seriously affected in case of a new eruption (**Fig. 12**). The eruptive record of San Miguel shows different episodes of unrest that are required to be analyzed in order to fully understand the periods of increased activity and their possible relation with the recorded monitoring parameters.

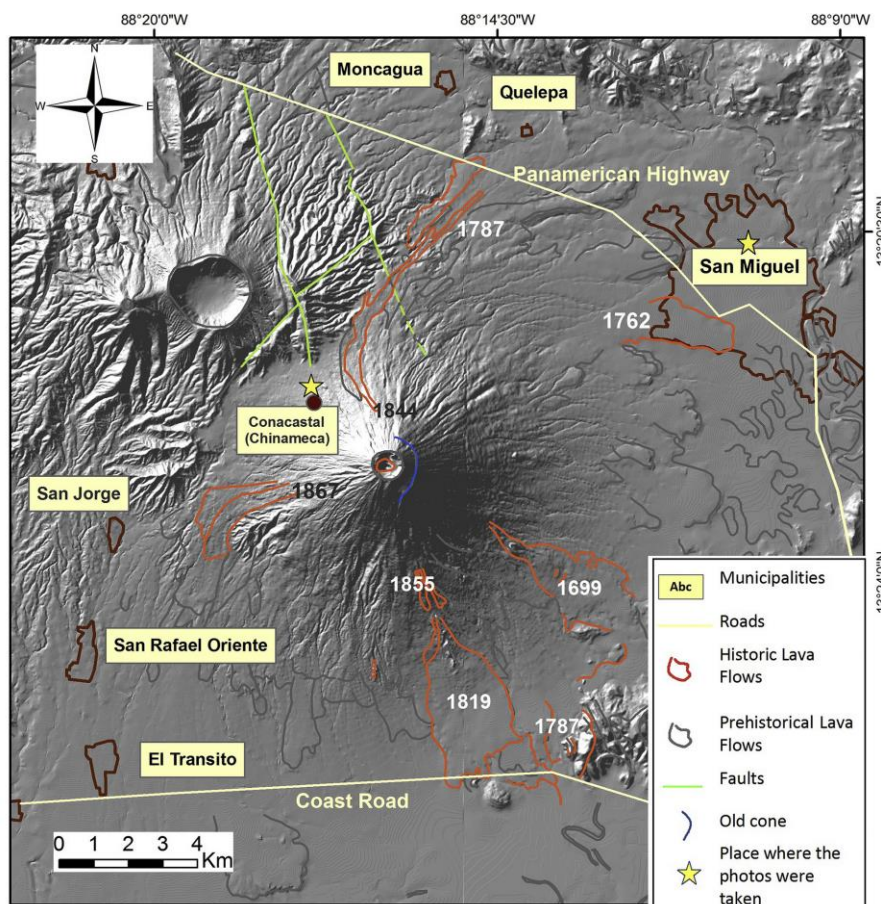


Figure 12. Shade relief map of San Miguel showing the main nearby cities and villages, and lava contours. Green lines are faults as mapped by the Observatorio Ambiental. Grey contours represent pre-historical lava flows. Red contours are historical lava flows with the year of eruption given, old crater is represented by the blue line (modified from Jiménez et al., 2018).

In the framework of the EUROVOLC project and, more specifically, thanks to the E-THA project (e-Tools for short-term volcanic Hazard Assessment) submitted to the 1st EUROVOLC Transnational Access Call by Dr. Diana Jimenez from the University of El Salvador, we used the QVAST tool (Bartolini et al., 2013) to upgrade the susceptibility map based on the information recorded during the different unrest phases (e.g., the location of the seismic events) and the ST-HASSET tool (Sobradelo et al., 2013; Sobradelo and Martí, 2015; Bartolini et al., 2016) to estimate the probability of occurrence of a particular eruptive scenario combining monitoring data with

information on past eruptions and unrest episodes. The ST-HASSET tool helped us to interpret the available information (monitoring and historical data) into a set of “precursory signals” that can be linked to a particular evolution of the unrest episode to identify the increase or decrease of the volcanic activity. This work will allow determining relevant parameters and corresponding critical levels, according to characteristics of volcanoes with high seismicity, frequent phreatic activity and with a very basic monitoring network. Results obtained can serve as a point of comparison for further studies in other El Salvador and central America volcanoes. The analysis for San Miguel volcano will represent a step forward to assess volcanic hazard in El Salvador and will contribute to considered to add the methodology as other tool for scientist at the National Observatory of Ministerio de Medio Ambiente y Recursos Naturales (OA-MARN) and for Civil Protection agency to face future volcanic crises in the country.

2.1.2 Scientific objectives

The main aim of this study has been to assess *the short-term volcanic hazard in San Miguel volcano applying a probabilistic approach able to incorporate monitoring information. The objective was to look for significant changes in the values measured during an episode of volcanic unrest with the purpose of identifying indicators across consecutive time intervals.* In order to achieve this, the planned work was divided into the following contingent objectives on the main one :

- a) Analyse reports or bulletins generated from 2002 to August 2019, in order to make a quality control and organize the data set. This step is very important as it is the starting point to define the time interval to be used in the study.
- b) Application of two e-tools HASSET and QVAST Short-Term.
- c) Conduct a retrospective analysis of the unrest episodes in 2013 preceding the 28th December eruption, with the purpose to define a guideline on how to manage the information generated by a monitoring network during the unrest phase of an ongoing crisis.

2.1.3 Methodology

For this study, monitoring data from 2002 to 2019 (e.g., Bonforte et al., 2016) and the long-term hazard assessment for San Miguel (Jiménez et al., 2018) were considered. San Miguel volcano has experienced several episodes of unrest with only very few culminating in an eruption. For each unrest period we estimated the evolution of different indicators, and calculated the probability of scenarios characterized by those indicators. Input information included: (i) 144 volcanic reports for San Miguel volcano in different formats; (ii) monitoring information (seismicity, Real-time Seismic-Amplitude Measurement (RSAM), SO₂ and superficial temperature) including data from 16 unrest episodes in the last 16 years and one eruption VEI 2 on December 29, 2013. The eruption was a vulcanian-type explosion that lasted 2.5 h and produced an ash plume with a maximum height of ~9 km (Scarlato et al., 2016). There were also other minor explosions with VEI 1. With the reports we constructed the monitoring data set and verified the coordinates systems on maps of LT special susceptibility. The same scenario (i.e. total seismicity, RSAM, shallow seismicity, and VT) was compared within each unrest period. Once we had the data set organized the next step was to learn from the two e-tools (HASSET & QVAST Short-Term) specifically designed for conducting probabilistic spatial and temporal analysis in volcanic hazard assessment. Considering the total unrest periods in our data set, as a first view we analysed each unrest separately. With this, we were comparing the same scenario (i.e. total seismicity, RSAM, shallow seismicity, and VT) in each unrest period. We observed that the estimated probability of an imminent eruption considering this scenario is more consistent with the behaviour in the next bulletin. For instance, in 2009 there were 2 unrest that did not culminate with an eruption. With the QVAST tool (Bartolini et al., 2014) we upgraded the susceptibility maps based on the monitoring information during each unrest. Hence, the previously defined probabilities of hosting a new vent changed based on the location of new seismicity – assuming that this provides an indication of magma movement and location. Complementary, with the ST-HASSET tool (Sobradelo and Martí, 2015; Bartolini et al., 2016) we have developed an event tree structure that uses a quantitative approach via Bayesian inference to assess the hazard of a particular volcanic scenario. We chose time windows of one year and six months and we are analysing separately different unrest periods.

2.1.4 Preliminary results

Preliminary results obtained indicate that the estimated probability of an imminent eruption considering this scenario is more consistent with the behavior in the next bulletin. For instance, in 2009 there were 2 unrest that ended in no eruption, in **Figure 13** we can see the probability estimated is less than 1%; unlike to take others as RSAM that in most of the cases overestimate probabilities (**Fig. 13**).

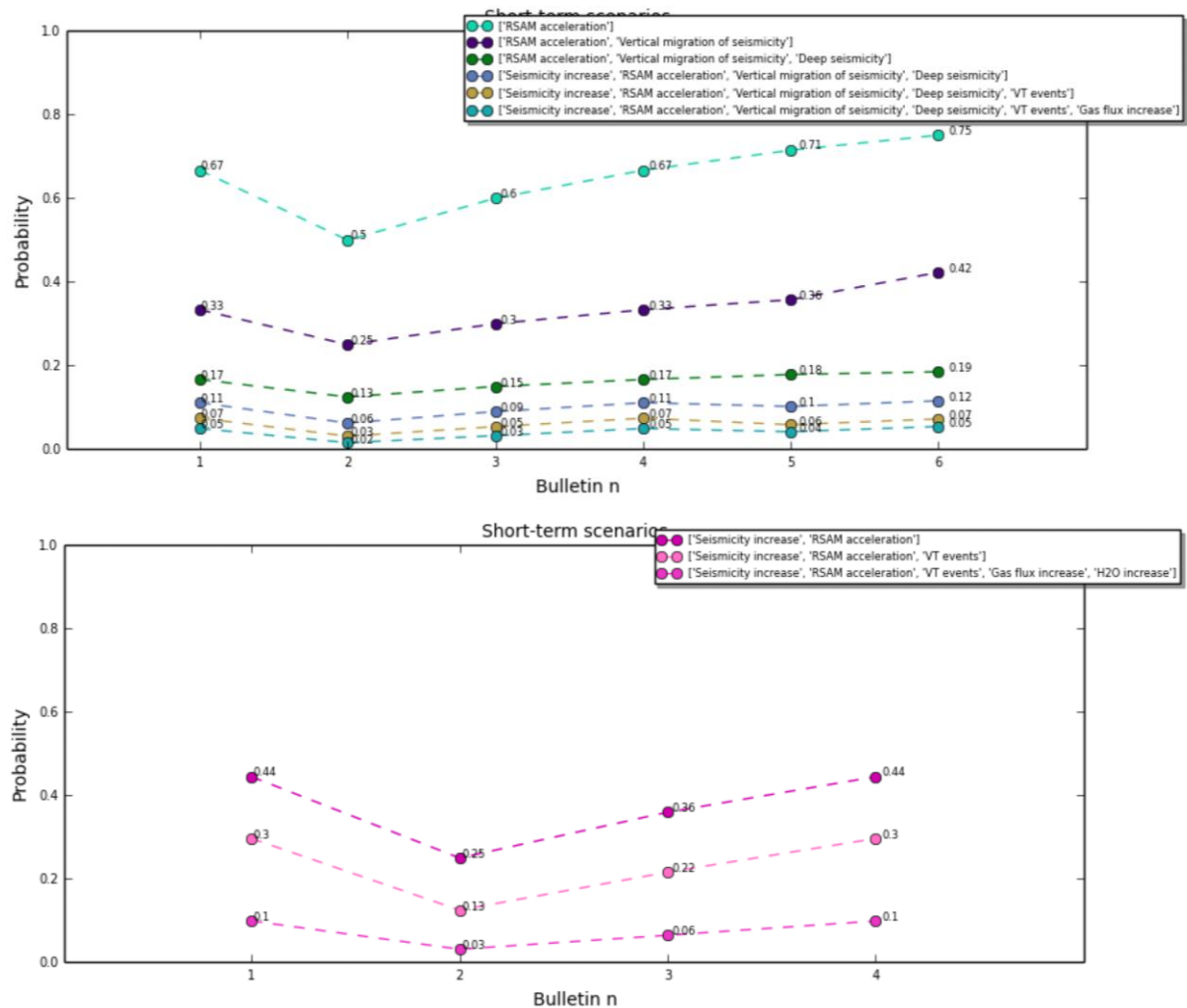


Figure 13: ST-HASSET the evolution of the unrest indicators for unrest in January 2014. Considering different scenarios (top), and RSAM scenarios and VT (bottom).

Currently, we are working on the preparation of a scientific paper. The results of this research have been partially presented at EGU 2020 scientific conference:

EGU2020-12669 | Displays | GMPV9.8. Transnational Access to on-site modelling resources and hazard assessment tools: Establishing the pillars of scientific collaboration. Adelina Geyer, Erika Ronchin, Diana Jimenez, Joan Martí, and Marc Martínez. Mon, 04 May, 16:15–18:00 | D1641

2.2 Application of CALPUFF model to Bárðarbunga eruption in 2014-2015, Iceland, to quantify gas hazard

The Holuhraun fissure eruption (Iceland) in 2014–2015, which originated from the Bárðarbunga volcanic system, was exceptional in several respects (**Figure 14**). It lasted 6 months and, throughout its duration, it released up to 9.6 Mt of SO₂ in the atmosphere. The main recorded hazard affecting the entire country over the 6 months was the constant presence of a low-level gas cloud that led to recurrent air pollution episodes. The Icelandic Meteorological Office responded to this human health hazard by (1) setting up a forecasting system to anticipate the distribution of SO₂ over Iceland and (2) preparing probabilistic hazard maps to support the decisions taken by the Icelandic Civil Protection in demarcating the accessible area around the eruption site. This paper introduced some technical aspects of the application of the CALPUFF numerical model (Barsotti & Neri 2008, Barsotti et al, 2008) to this eruption like the SO₂ dispersal forecasting setup, the volcanic source numerical description, and the Monte Carlo procedure adopted for the creation of the probabilistic hazard maps. CALPUFF-based maps were created in January 2015, when the eruption was still ongoing, with the assumption that the eruption would be continuing with the same intensity. Maps for the entire country and for a smaller domain were produced, the latter showing the likelihood to exceeding an hourly concentration of 2600 µg/m³ (1 ppm) of SO for the spring season, a level chosen by the Icelandic Civil Protection for the delineation of the area of restricted access around the eruption site. As during the eruption there was no time for a rigorous evaluation of the model accuracy, we then undertook a retrospective analysis of CALPUFF model performance comparing the forecasted hourly SO₂ concentration with real-time measurements at key-sites.

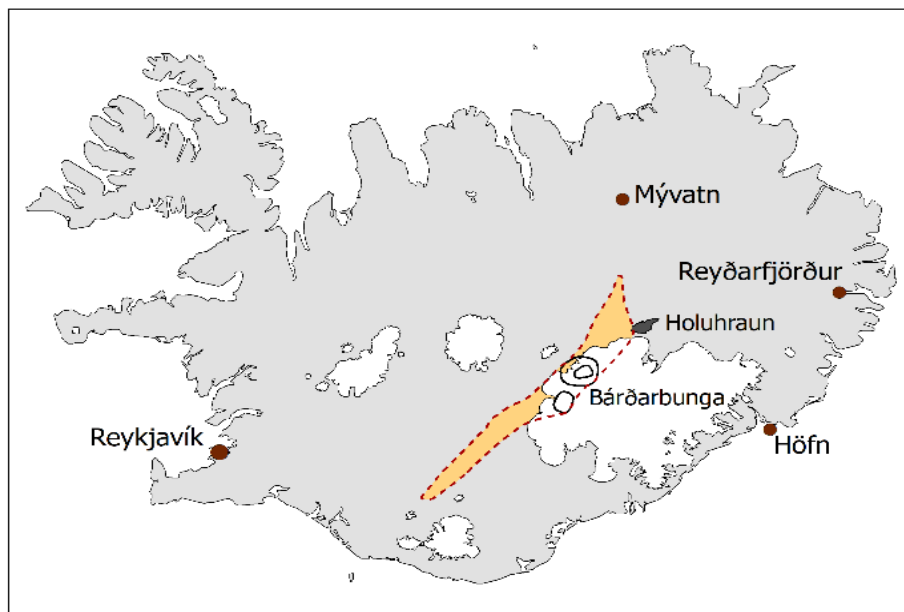


Figure 14 Map showing the Bárðarbunga volcanic system extension (orange area) with the central volcano (black circles), the location of the Holuhraun lava flow field (black area), and the four locations used to validate the model performances (dark red dots).

The model did reproduce the hourly observations (the maximum within a 24-running window) with a level of agreement of 50.6% in Mývatn (85 km from the eruption site) and 50.4% in Reykjavík (258 km), when instances of null pairs have been removed. In Mývatn, the model overestimated the concentration more than 22% of the time. In Höfn (104 km), the model accuracy is 81.7% and occurrences of underestimation are higher than 11% of the time. In Reyðarfjörður (at 124 km), the model accuracy is assessed to be 82.7% and the model overestimates occurring 15.1% of the time (see **Figure 15**). Possible explanations for the observed mismatch between model results and measurements include the spatial resolution of the meteorological data field, the capability to reproduce chemical reactions of SO₂ in the atmosphere, and the reduced extension of the numerical domain. In addition, the model performance is strongly dependent on the source descriptors (e.g., strength of the SO₂ flux and injection height) that, in this contribution, have been kept constant over long periods—neglecting, in this way, the natural

variability of a dynamic emission of SO₂. This consideration points toward the need of frequent and high-quality observation data for the initialization of dispersal numerical models. In light of this retrospective analysis, the probabilistic hazard maps (**Figure 16**) possibly over-estimated the area exposed to high levels of SO₂ concentration. All the same, this paper reports on how quantitative probabilistic hazard mapping can be used for mitigating the health risk of volcanic SO₂ emissions during a volcanic crisis to the benefit of operational hazard monitoring in support of an effective crisis response.

		Reyðarfjörður				Mývatn			
Modelled SO ₂ concentration (µg/m ³)	>2600	0	0	0	0	(0.7%) 24	(0.6%) 18	(0.2%) 7	0
	600-2600	(7.1%) 214	(0.1%) 2	(1.1%) 32	0	(10.5%) 340	(1.5%) 48	(5.4%) 174	0
	350-600	(7.9%) 236	(0.4%) 13	(0.2%) 6	0	(8.5%) 276	(1.8%) 58	(2.3%) 74	0
	<350	(81.2%) 2435	(0.8%) 23	(1.3%) 39	0	(65.1%) 2109	(1.1%) 36	(2.4%) 77	0
		Höfn				Reykjavík			
Modelled SO ₂ concentration (µg/m ³)	>2600	0	0	0	0	0	0	0	0
	600-2600	(1.7%) 38	(3.8%) 87	(6.2%) 142	(0.9%) 21	(0.8%) 28	(0.7%) 24	0	0
	350-600	(1.8%) 40	(1.6%) 36	(3.9%) 89	(0.1%) 3	(2.4%) 84	(0.9%) 31	(0.5%) 19	0
	<350	(73.9%) 1684	(2.0%) 45	(4.2%) 95	0	(90.6%) 3153	(3%) 103	(1.1%) 38	0
		Measured SO ₂ concentration (µg/m ³)				Measured SO ₂ concentration (µg/m ³)			
		<350	350-600	600-2600	>2600	<350	350-600	600-2600	>2600

Figure 15: Overview of the comparison between the hourly (maximum over 24 h) modeled SO₂ concentration at ground level and the concentrations measured each hour by the monitoring stations operated by EAI by using confusion matrices for four locations.

Four main points can be summarized in light of this study:

- To our knowledge, this is the first time that the CALPUFF model has been used to simulate the dispersal of SO₂ originating from volcanic source and we can here confirm it to be a valid tool for daily forecasting of SO₂ concentration over Iceland and for providing air pollution warnings during volcanic crises.
- Long-lasting eruptions are cases of eruptive scenarios for which a short-term probabilistic hazard assessment is desirable and achievable.
- The quantification of performance metrics (recall, precision, and accuracy) reveals that the quality of the model results strongly depends on the source-receptor distance as well as on the level of concentration considered. Important elements that need to be investigated to fully evaluate the capability of CALPUFF in modeling near- and far-field SO₂ dispersal are (1) the temporal evolution of model source conditions; (2) the role of chemical reactions and wet deposition, (3) the result of using high spatial resolution meteorological data, and (4) the effect of increasing the size of computational spatial domain to take into account the arrival of mature plumes in the modeled air space.
- Our retrospective CALPUFF performance analysis revealed that the model often overestimated at the location closest to the eruption site. As a consequence, the seasonal SO₂ hazard map used by the Icelandic Civil Protection to designate the restricted areas in late February 2015 was a conservative assessment.

Fundamentally, hazard assessment can be best translated into mitigation actions when the scientific community works alongside the civil protection authorities prior to and during volcanic crises. This is the blueprint that we have followed, and demonstrated, here.

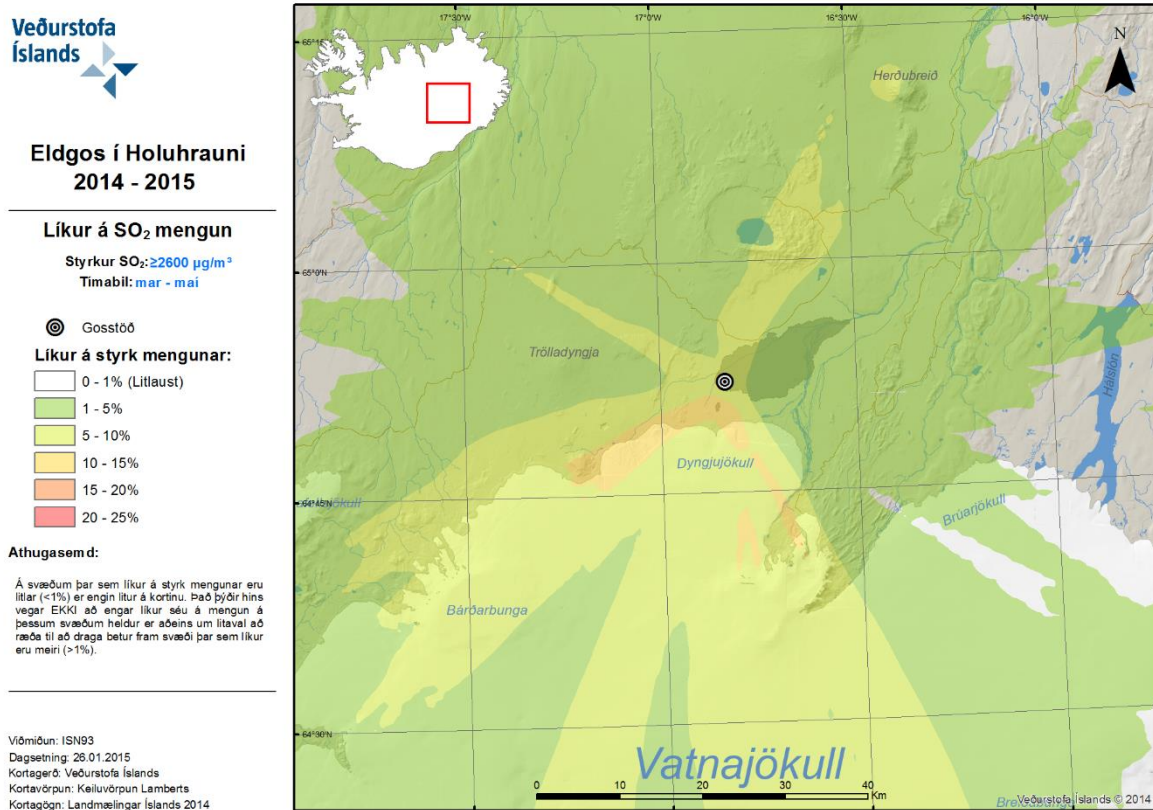


Figure 16: Example of probabilistic hazard maps for SO₂ concentration exceeding 2600 µg/m³ in the spring period. Similar maps were produced for different thresholds and temporal windows at the time of the eruption.

The results of this study are included in a published paper:

Barsotti, S. Probabilistic hazard maps for operational use: the case of SO₂ air pollution during the Holuhraun eruption (Bárðarbunga, Iceland) in 2014–2015. *Bull Volcanol* **82**, 56 (2020). <https://doi.org/10.1007/s00445-020-01395-3>

See the appendix for a picture of the front cover (**Figure A.3**).

2.3 GIS-based risk analysis for evacuation modelling at Stromboli

2.3.1. Introduction

In Bonilauri et al (2021) (Bonilauri E, Harris A, Morin J, et al., 2021. Tsunami evacuation times and routes to safe zones: a GIS-based approach to tsunami evacuation planning on the island of Stromboli, Italy. *Journal of Applied Volcanology* 10:4, <https://doi.org/10.1186/s13617-021-00104-9>, see the appendix for a picture of the front cover in **Figure A.4**), we developed a new method based on Geographical Information System (GIS) methodology to generate large-scale and individual building evacuation plans for the study case of Stromboli. Our method is built on the models of Péroche (2016) and Leone et al. (2018), to evaluate the best horizontal evacuation of pedestrians from a populated coastline in case of a locally originated volcanic tsunami for which the response time is low. On the island of Stromboli, on December 30, 2002, two landslides were triggered at the Sciara del Fuoco, the first at 13:15 (local time) and the second at 13:22. They generated two tsunamis 7 min apart with a maximum run-up of 10.9 m and affected the entire coastline in less than 4 min (Tinti et al. 2006a; Tinti et al. 2006b). The first tsunami was essentially due to a submarine landslide and involved $20 \times 10^6 \text{ m}^3$ of material (Chiocci et al. 2003). The second tsunami was caused by a purely sub-aerial landslide that broke off at about 500 m a.s.l and involved a volume of material of between 4 and $9 \times 10^6 \text{ m}^3$ (Tinti et al. 2006b). **Fig. 17** gives the run-up area of these two tsunamis obtained from post-event surveys (Maramai et al. 2005; Tinti et al. 2006a).

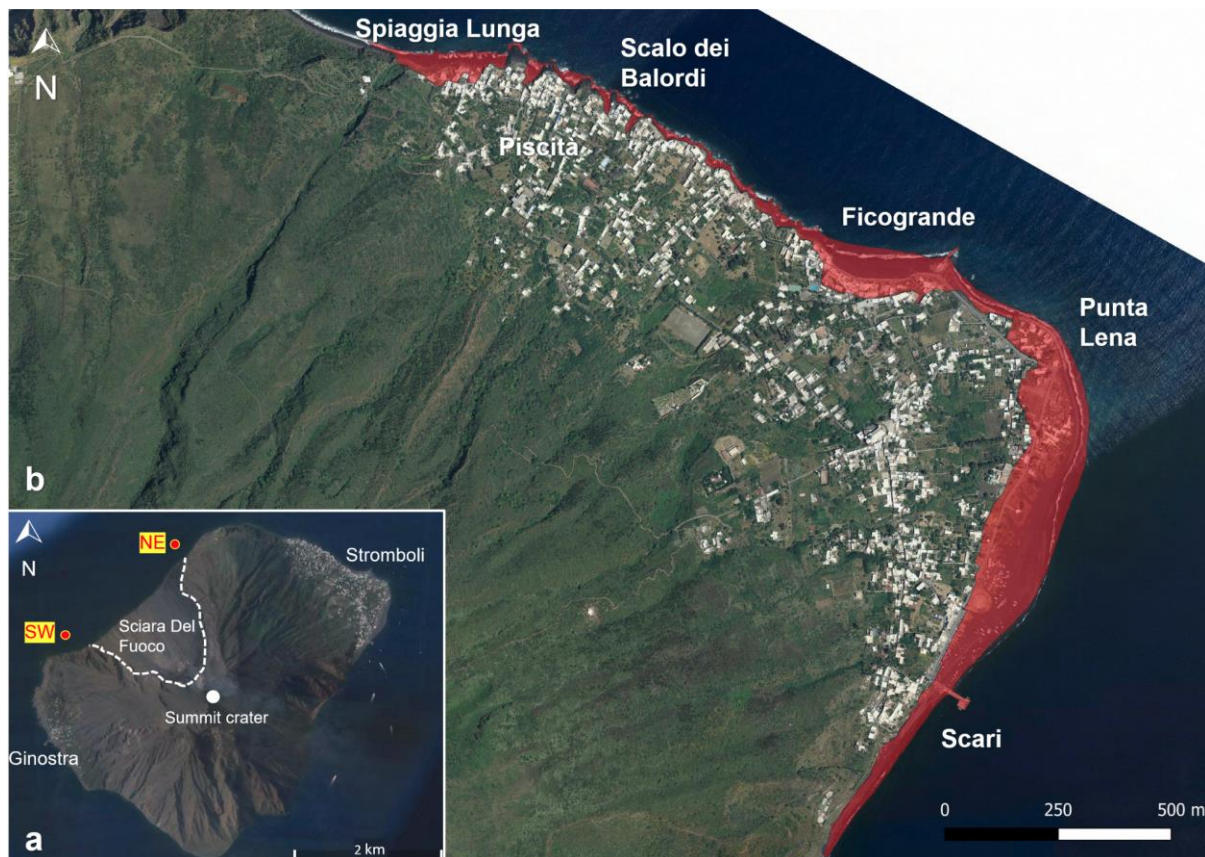


Figure 17. a) Map of the island of Stromboli with Stromboli and Ginostra villages, the Sciara del Fuoco, and the two sea floor tsunami sensors located to the Northeast and Southwest of the Sciara del Fuoco. b) Map of Stromboli village with the zone impacted by 2002-tsunami. From Bonilauri et al. 2021.

In 2019, on July 3 and August 28, two paroxysms occurred releasing an ash plume several kilometres high and producing pyroclastic flows on the Sciara del Fuoco (Global Volcanism Program 2019). Seafloor pressure sensors at the foot of the Sciara del Fuoco recorded a tsunami with an amplitude of 40 to 20 cm (data transmitted directly to the LGS - Laboratorio Geofisica Sperimentale - Università di Firenze, Florence, Italy). The sensors are

connected to a siren warning system in the village of Stromboli. During the August 28 paroxysm, the sirens were triggered manually 15 seconds after the wave was formed and 75 seconds after the explosion (Lacanna and Ripepe in prep.). The reactions of tourists and people on the beaches were very confused. This experience argues for the need for a well-defined evacuation plan with clearly marked evacuation routes and safe locations. The 2002 and 2019 tsunami scenarios are currently used by civil protection as an evacuation scenario.

2.3.2. Methodology

The GIS methodology was set up in a five-step process on QGIS software to allow the generation of the key product: an evacuation route map and evacuation time matrix (Bonilauri et al. 2021). Step 1 consisted of the evacuation area delineation. We defined three zones: a red zone which represents the area to be evacuated in the case of a December 2002-type event for which we have 4 min of warning; a yellow zone which is a possible error margin; and a green zone which is the “safe” zone and starts above the 15 m contour. High-stake areas were considered in Step 2, where all buildings of the red zone were analysed in detail because of their high exposure in the event of a future tsunami. This analysis was carried out using a field survey form where we determined: ease of evacuation of a building, location and size of windows and doors for each floor, accessibility of the roof, presence of shutters and their type, and presence of gates and steps. In Step 3, we built the road network and estimated the evacuation speed of evacuees according to the slope of the terrain (Péroche 2016). Each road section was assigned a speed reduction coefficient according to its nature: two-lane roads, single-lane roads, and paths. Step 4 considered the number of evacuees to assess the load of the evacuation network in terms of congestion. Two types of evacuation scenarios were chosen for the red zone: an individual evacuation of each building and a large-scale evacuation of tourist gathering. To reach the green zone, evacuees from the entire area must pass through a refuge area entry point (RAEP). In step 5, we calibrated the evacuation simulation with the QGIS plugin QNEAT3 and with a Python script and obtained all the fastest evacuation routes to the safe area and associated times.

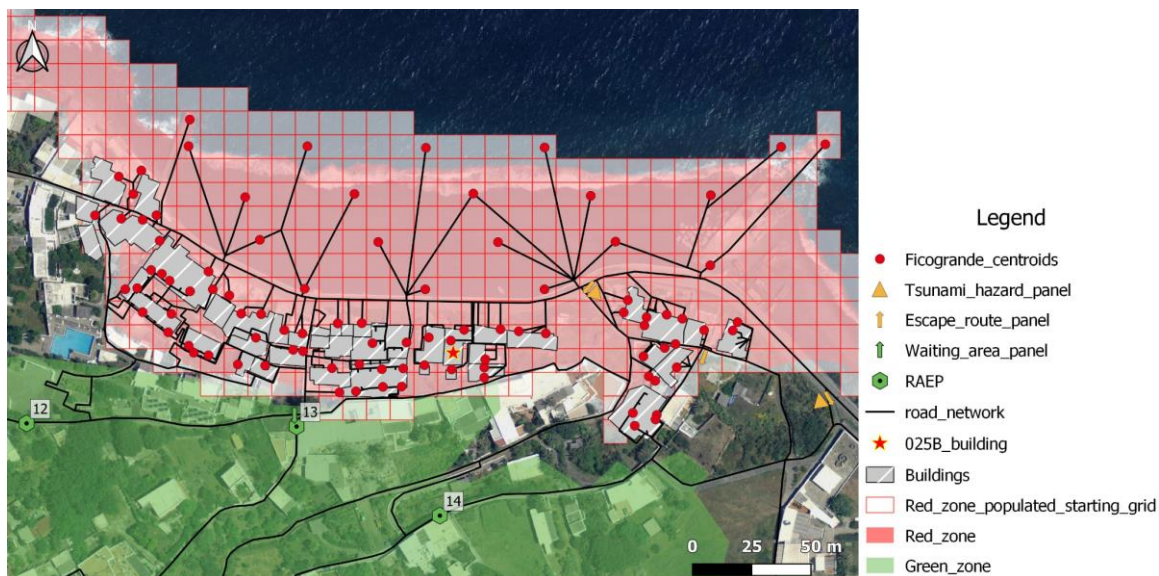


Figure 18 Evacuation routes from all starting centroids (Bonilauri et al. 2021).

2.3.3. Modelling results

Our initial aim was to implement and test the methodology, so we focused on a single control area that contained all the key elements of the evacuation scenario and was representative of the content of the GIS for the whole risk area: the Ficogrande area. This area was particularly affected by the December 2002 tsunami, where water and entrained debris reached a height of 10 m causing significant material damage to buildings (Tinti et al. 2006a). The topography is also very steep, which makes evacuation even more difficult to organise. **Fig. 18** shows all possible evacuation routes from all possible starting points in the Ficogrande area.

We used this road network to estimate the evacuation time and the optimal evacuation route (**Fig. 19**). The evacuation time calculations only consider the registered speeds of the road network and do not include the time needed to exit the building or the reaction time of evacuees. Congestion phenomena can also not be considered by the QNEAT3 plugin of QGIS. The distribution of individuals between the different Refuge Area Entry Point is not homogeneous and will create a much larger group of people at the RAEP13 and can therefore be reported as a potential bottleneck (Ma et al. 2014). A tsunami generated by a landslide at the foot of the Sciara del Fuoco will arrive at Ficogrande in less than 4 min after the siren alert. It can be seen here that of the 94 starting points, 73 can be evacuated in less than 4 min and therefore this means that 21 points are not (Bonilauri et al 2021).

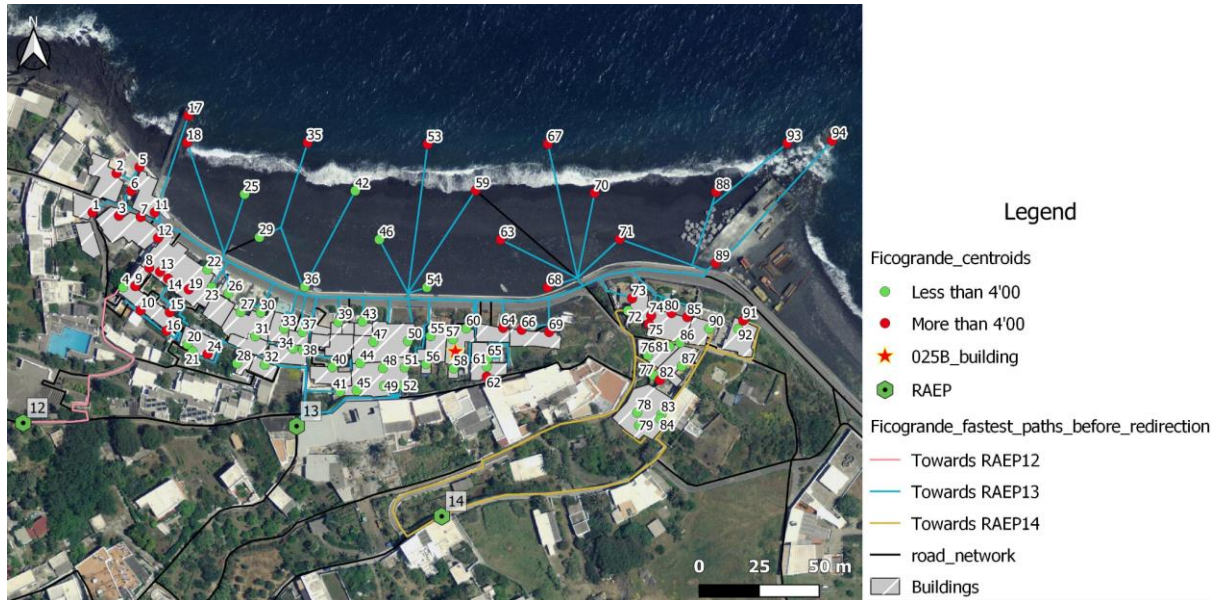


Figure 19 Possibility of evacuating in less than 4 min in Ficogrande (Bonilauri et al. 2021).

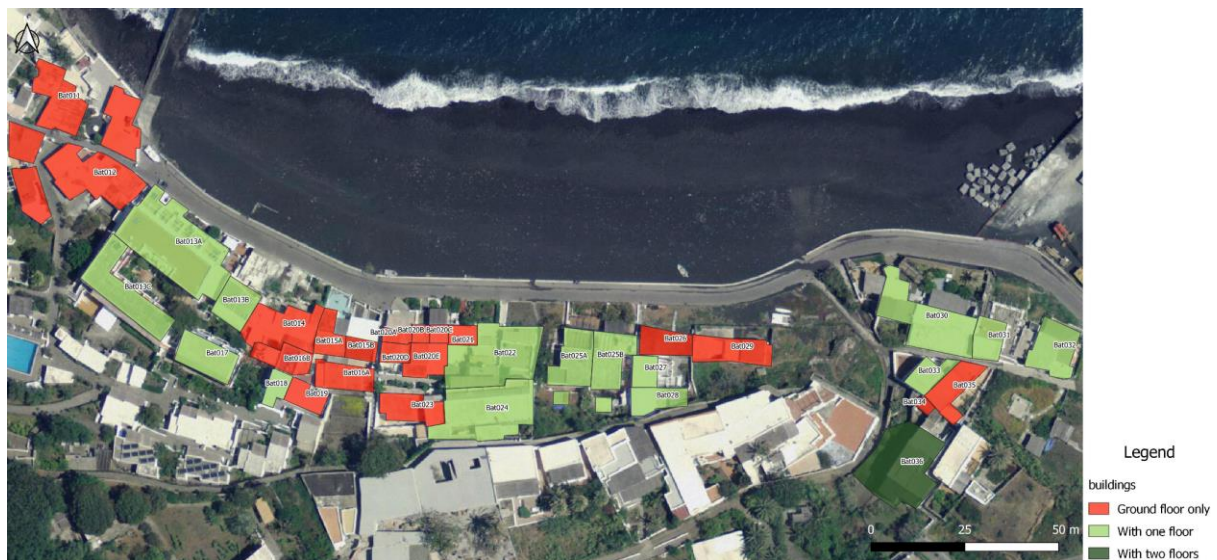


Figure 20 Consideration of vertical evacuation (Bonilauri et al. 2021).

Reaching the safe zone in time for several starting points is not always possible. Taking refuge on the roof if the roof level remains below 10 m is not a good solution because the roof might be inundated by the tsunami. However, in cases where the roof height attains the 10 m level (corresponding to the roof of the first or second floor depending on the location), the roof could be used as a last resort option for a vertical evacuation shelter. We generated maps identifying these possible shelter options (**Fig. 20**). However, this option should only be considered as a last resort due to the risk of building failure (Nakano 2010).

We used the detailed building field surveys to develop individual evacuation plans for each building in the red zone (**Fig. 21**). To design these plans, we followed the role, design, and use of standard fire evacuation plan symbols as displayed on hotel room doors (Kobes et al. 2010; Wang et al. 2014). The aim is to ensure that the maps are not shocking, but rather deal with an event that can happen and for which we need to prepare.

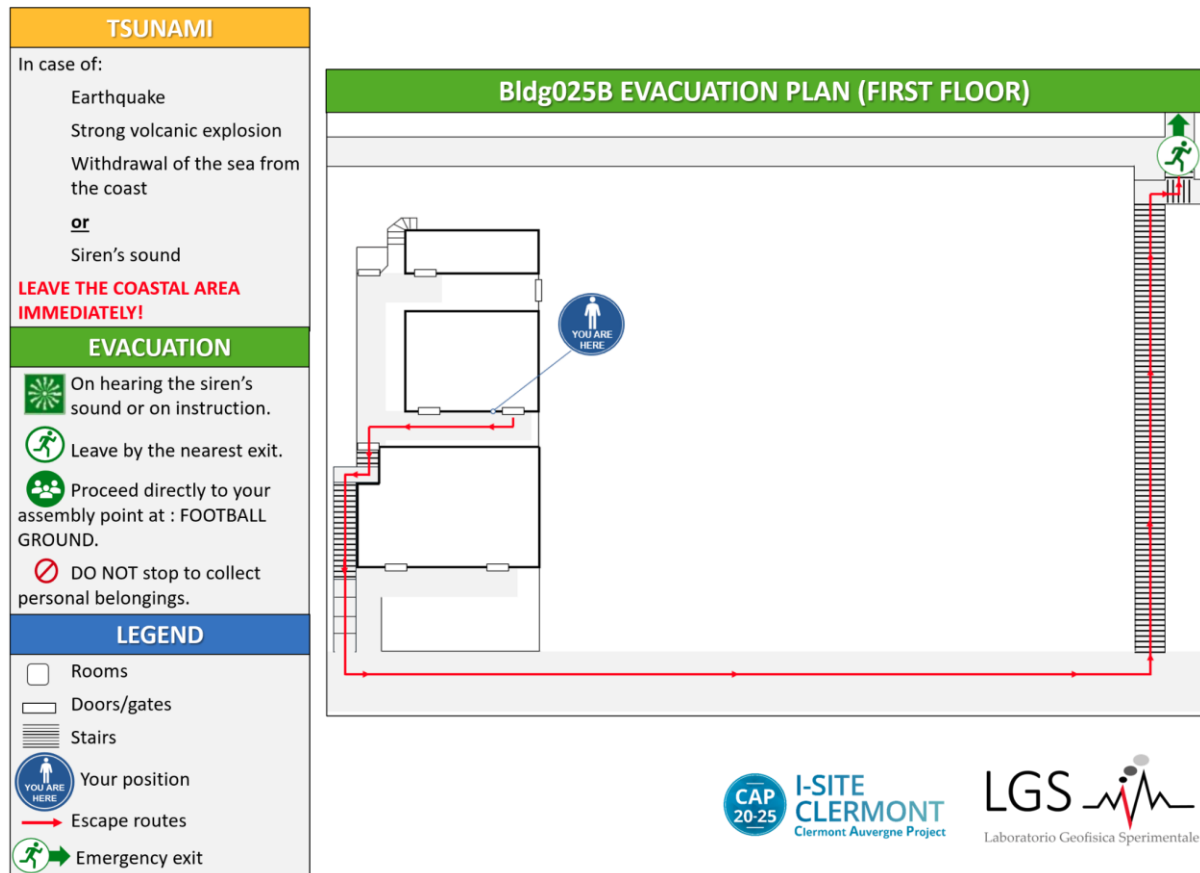
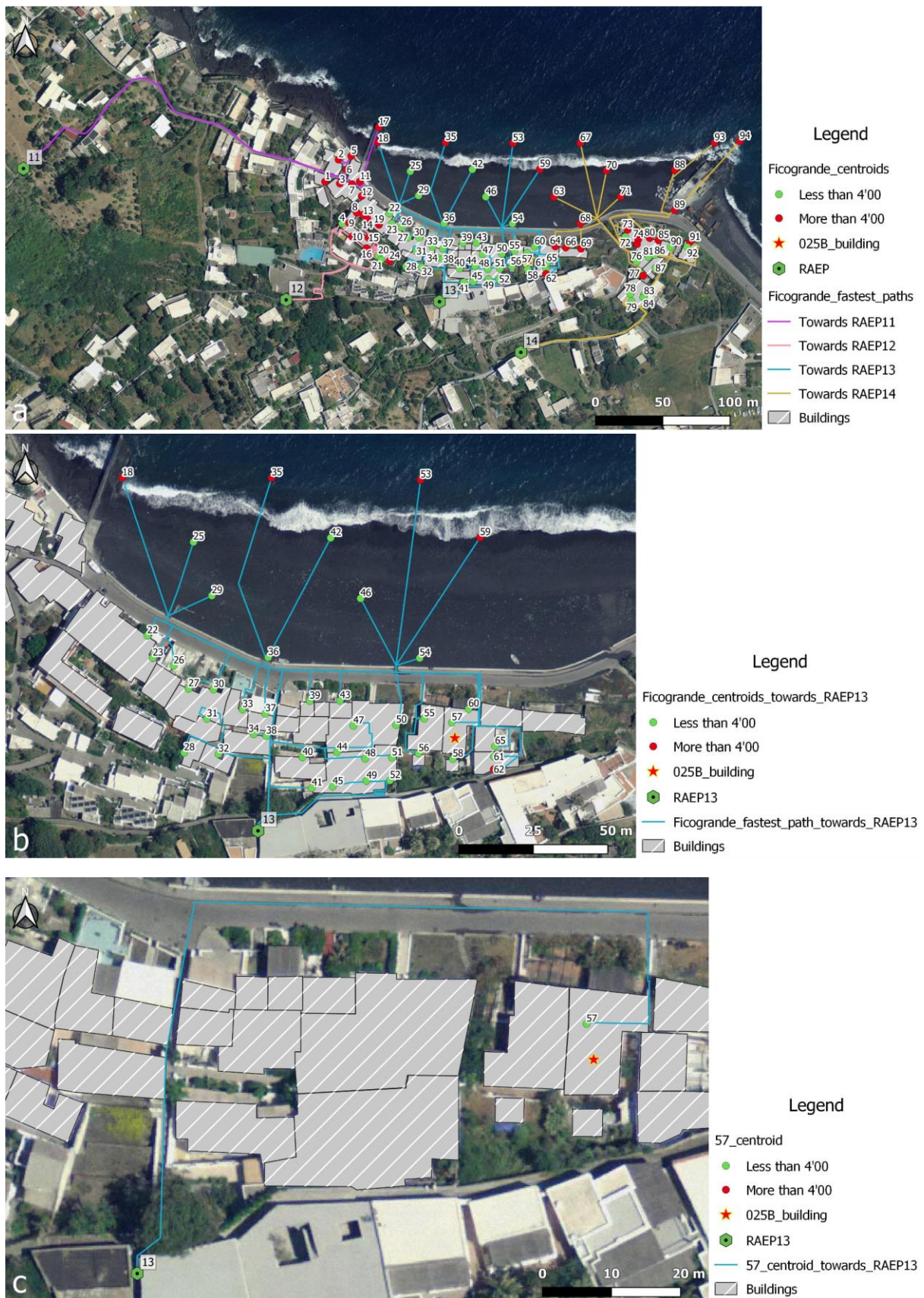


Figure 21 Personalised evacuation plan for building 025B (Bonilauri et al. 2021).

2.3.4. Considerations

In the study case of the island of Stromboli, the priority area for evacuation was estimated from the 2002 scenario. The 2002 tsunami was the largest tsunami of the last century and has been particularly well-analysed (Chiocci et al. 2008). However, the yellow zone added allows for a potentially larger event to be considered. Evacuation modelling in the Ficogrande area shows that most points are evacuated to RAEP13 and that most points can be evacuated in 4 min (Bonilauri et al. 2021). Some points had to be redirected to other RAEPs, however, to minimise the effect of a bottleneck at RAEP13 (**Fig. 22a**). Our model can therefore be considered as the fastest possible evacuation time when optimal traffic and reaction conditions are adopted. It can also identify potential improvements to the evacuation road network and make recommendations to place new signage and vertical evacuation structures. Our methodology allowed us to create three scales of evacuation maps. The first scale is zonal and shows evacuations from all departure points to all existing RAEPs in a given area (**Fig. 19a**). The second scale is for all departure points that go to one and the same RAEP (**Fig. 22b**). The third scale concerns each individual door, without any other door being indicated, to maximise clarity (**Fig. 22c**).

The addition of specific exit signs and personalised evacuation plans (cf **Fig. 21**) that would direct guests out of the hotel and to the nearest RAEP would make evacuation easier in case of a tsunami. According to our



modelling, at least 7 min and 6 s are needed to evacuate the Ficogrande area without considering congestion and bottleneck phenomena and without reaction time. A minimum of 10 minutes' warning seems to be essential to consider a full evacuation of the area. Such a warning period would also allow for uniformity of choice in evacuation routes so that one route does not suffer congestion or bottleneck effects.

Our maps can be followed as a guide as to the optimal route to choose and the shelter point to reach. As our methodology is applicable on a large spatial scale, it could be used for any island population exposed to a tsunami, especially on small volcanic islands which, like Stromboli, are close to the tsunamigenic source.

3 – Development of new open tools for volcanic hazard assessment

3.1 VIGIL: an automatized probabilistic volcanic gas dispersion model

The DISGAS application at La Soufrière de Guadeloupe (Section 1.1) prompted the development of VIGIL (Volcanic Gas dispersion modelling), a new tool designed for managing the complex and time-consuming simulation workflow involved in probabilistic applications of gas dispersion modelling. The development of VIGIL was carried out by the British Geological Survey in collaboration with INGV and funded by the UK National Capability budget (Innovation Flexible Fund). The tool was recently made available on the BGS Github repository (<https://github.com/BritishGeologicalSurvey/VIGIL>), and a paper presenting it will soon be submitted.

VIGIL acts as a wrapper around two gas dispersal simulation tools: DISGAS (Costa et al. 2016) and TWODEE (Folch et al. 2009). In the framework of VIGIL development, both codes have been recently upgraded and made available on the INGV repository, together with the diagnostic wind model DIAGNO (Douglas et al. 1990). Specifically:

DISGAS v2.1: <http://datasim.ov.ingv.it/models/d disgas.html>

TWODEE v2.3: <http://datasim.ov.ingv.it/models/twodee.html>

DIAGNO v1.1.1: <http://datasim.ov.ingv.it/models/diagno.html>

DISGAS is used to simulate the passive dispersal of dilute gases (e.g. fumaroles) by solving the advection-diffusion equation in the atmosphere. TWODEE, on the other hand, is a model for heavy gas flows (e.g. CO₂) by means of the shallow-water model.

VIGIL is designed to control the three main steps characterizing a typical gas dispersal simulation and simplify the management of the numerous simulations required for probabilistic volcanic hazard applications. The three steps are:

- meteorological data retrieval and processing. Reanalysis from ERA5 (Copernicus Climate Change Service, 2017) and forecast from NOAA-NCEP Global Forecast System (<https://www.ncdc.noaa.gov/data-access/model-data/model-datasets/global-forecast-system-gfs>) can be used for reanalysis and forecast modes, respectively. In reanalysis mode it is possible to download weather data from N days, hence allowing to explore the meteorological variability in a probabilistic modelling application.
- meteorological data are first processed with DIAGNO to obtain the wind field in the computational domain and on a Digital Elevation Model of the terrain. Then VIGIL launches the forecast simulation or the N reanalysis simulations with DISGAS or TWODEE, depending on the application selected by the user. The simulations can be run in parallel. The variability of the gas source number, location and strengths can also be explored.
- Model results are then processed to produce useful outputs including plots of gas concentration at selected time steps and vertical levels. In this stage, in case of a probabilistic modelling application, it is possible to combine the outputs to build empirical cumulative density functions, which can then be interrogated by the user to produce, e.g., concentration maps at specific exceedance probabilities.

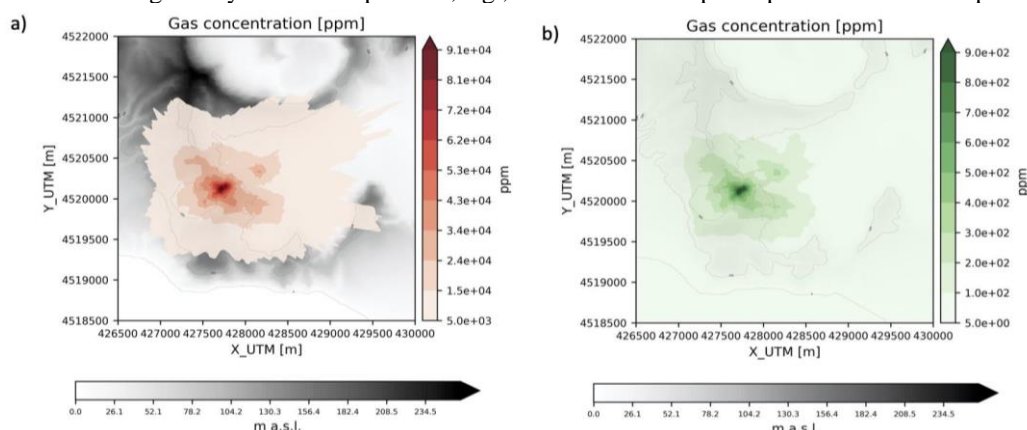


Figure 23 - Examples of probabilistic concentration maps from Solfatara volcano (Campi Flegrei, Italy). The gas concentration (in ppm) is shown at 1.5 m above the ground, after 24 hours. a) CO₂ concentration for 250 days corresponding to the 5% exceedance probability of the whole simulation dataset; b) H₂S concentration for 250 days corresponding to the 5% exceedance probability of the whole simulation dataset.

VIGIL is in continuous development with new functionalities and options to further improve its capabilities already planned in the next future. In **Figure 23** two examples of the post-processing application are reported for the Solfatara volcano (Campi Flegrei, Italy) case study: in particular, the production of the probabilistic concentration maps corresponding to the 5% exceedance probability of the whole simulation dataset.

References

- Allard, P., Aiuppa, A., Beauducel, F., Gaudin, D., Di Napoli, R., Calabrese, S., Parello, P., Crispi, F., Hammouya, G., Tamburello, G., 2014. Steam and gas emission rate from La Soufriere volcano, Guadeloupe (Lesser Antilles): implications for the magmatic supply during degassing unrest. *Chemical Geology*, 384, 76-93.
- Barsotti S, Neri A (2008) The VOL-CALPUFF model for atmospheric ash dispersal: 2. Application to the weak Mount Etna plume of July 2001. *J Geophys Res Solid Earth* 113(B3)
- Barsotti S, Neri A, Scire J (2008) The VOL-CALPUFF model for atmospheric ash dispersal: 1. Approach and physical formulation. *J Geophys Res Solid Earth* 113(B3)
- Barsotti, S. Probabilistic hazard maps for operational use: the case of SO₂ air pollution during the Holuhraun eruption (Bárðarbunga, Iceland) in 2014–2015. *Bull Volcanol* **82**, 56 (2020). <https://doi.org/10.1007/s00445-020-01395-3>
- Bartolini, S., Cappello, A., Martí, J., and Del Negro, C. (2013) QVAST: a new Quantum GIS plugin for estimating volcanic susceptibility, *Nat. Hazards Earth Syst. Sci.*, 13, 3031–3042, <https://doi.org/10.5194/nhess-13-3031-2013>.
- Bartolini, S., Sobradelo, R., and Martí, J. (2016) ST-HASSET for volcanic hazard assessment: A Python tool for evaluating the evolution of unrest indicators, *Comput. Geosci.*, 93, 77–87, <https://doi.org/10.1016/j.cageo.2016.05.002>
- Baxter PJ, Boyle R, Cole P, Neri A, Spence R, Zuccaro G (2005) The impacts of pyroclastic surges on buildings at the eruption of the Soufrière Hills volcano, Montserrat. *Bull Volcanol* 67:292–313. <https://doi.org/10.1007/s00445-004-0365-7>
- Baxter PJ, Aspinall WP, Neri A, Zuccaro G, Spence RJS, Cioni R, Woo G (2008) Emergency planning and mitigation at Vesuvius: a new evidence-based approach. *J Volcanol Geotherm Res* 178:454–473 <https://doi.org/10.1016/j.jvolgeores.2008.08.015>
- Baxter PJ, Jenkins S, Seswandhana R, Komorowski JC, Dunn K, Purser D, Voight B, Shelley I (2017) Human survival in volcanic eruptions: thermal injuries in pyroclastic surges, their causes, prognosis and emergency management. *Burns* 43:1–19. <https://doi.org/10.1016/j.burns.2017.01.025>
- Biass, S., Falcone, J. L., Bonadonna, C., Di Traglia, F., Pistolesi, M., Rosi, M., and Lestuzzi, P., 2016. Great Balls of Fire: A probabilistic approach to quantify the hazard related to ballistics—A case study at La Fossa volcano, Vulcano Island, Italy. *J. Volcanol. Geotherm. Res.*, 325, 1-14.
- Bonforte, A., Hernandez, D. A., Gutiérrez, E., Handal, L., Polío, C., Rapisarda, S., and Scarlato, P.: The unrest of the San Miguel volcano (El Salvador, Central America): installation of the monitoring network and observed volcano-tectonic ground deformation, *Nat. Hazards Earth Syst. Sci.*, 16, 1755–1769, <https://doi.org/10.5194/nhess-16-1755-2016>, 2016.
- Bonilauri E, Harris A, Morin J, et al (2021) Tsunami evacuation times and routes to safe zones: a GIS-based approach to tsunami evacuation planning on the island of Stromboli, Italy. *Journal of Applied Volcanology* 10:4. <https://doi.org/10.1186/s13617-021-00104-9>
- Boudon G, Le Friant A, Komorowski J-C et al (2007) Volcano flank instability in the Lesser Antilles Arc: diversity of scale, processes, and temporal recurrence. *J Geophys Res*, SE 112:B08205. <https://doi.org/10.1029/2006JB004674>
- Boudon G., Komorowski J-C., Villemant B, Semet M.P. (2008). A new scenario for the last magmatic eruption of La Soufrière de Guadeloupe (Lesser Antilles) in 1530 A.D.: evidence from stratigraphy, radiocarbon dating and magmatic evolution of erupted products. *J. Volcanol. Geotherm. Res.*, 178:474-490.

- Calder E, Wagner K, Ogburn SE (2015) Volcanic hazard maps. In: Loughlin SC, Sparks S, Brown SK et al (eds) *Global Volcanic Hazards and Risk*. Cambridge University Press, Cambridge, pp 335–342. <https://doi.org/10.1017/CBO9781316276273.022>
- Carcano S, Bonaventura L, Esposti Ongaro T, Neri A (2013) A semi-implicit, second-order-accurate numerical model for multiphase underexpanded volcanic jets. *Geosci Model Dev* 6:1905–1924. <https://doi.org/10.5194/gmd-6-1905-2013>
- Chiocci F, Bosman A, Romagnoli C et al (2003) The December 2002 Sciara del Fuoco (Stromboli Island) submarine landslide: a first characterization, p 12069
- Chiocci F, Romagnoli C, Tommasi P (2008) The Stromboli 2002 tsunamigenic submarine slide: characteristics and possible failure mechanisms. *J Geophys Res* 113: [https://doi.org/10.1029/2007JB005172\(B10\)](https://doi.org/10.1029/2007JB005172(B10))
- Copernicus Climate Change Service (C3S), 2017. ERA5: Fifth generation of ECMWF atmospheric reanalyses of the global climate. Copernicus Climate Change Service Climate Data Store (CDS). <https://cds.climate.copernicus.eu/cdsapp#!/home>.
- Costa A., Macedonio G., 2016. DISGAS: A model for passive DISpersion of GAS, Rapporti tecnici INGV, N. 332, Istituto Nazionale Di Geofisica e Vulcanologia, Italy.
- Costa A, Suzuki YJ, Cerminara M, Devenish BJ, Ongaro TE, Herzog M, van Eaton AR, Denby LC, Bursik M, de' Michieli Vitturi M, Engwell S, Neri A, Barsotti S, Folch A, Macedonio G, Girault F, Carazzo G, Tait S, Kaminski E, Mastin LG, Woodhouse MJ, Phillips JC, Hogg AJ, Degruyter W, Bonadonna C (2016) Results of the eruptive column model inter-comparison study. *J Volcanol Geotherm Res* 326:2–25. <https://doi.org/10.1016/j.jvolgeores.2016.01.017>
- Douglas, S.G., Kessler, R.C., and Carr, E.L., 1990. User's guide for the Urban Airshed Model. Volume 3. User's manual for the Diagnostic Wind Model (No. PB-91-131243/XAB). Systems Applications, Inc., San Rafael, CA (USA).
- Esposti Ongaro T, Neri A, Todesco M, Macedonio G (2002) Pyroclastic flow hazard assessment at Vesuvius (Italy) by using numerical modeling II. Analysis of flow variables. *Bull Volcanol* 64:178–191. <https://doi.org/10.1007/s00445-001-0190-1>
- Esposti Ongaro T, Cavazzoni C, Erbacci G, Neri A, Salvetti MV (2007) A parallel multiphase flow code for the 3D simulation of explosive volcanic eruptions. *Parallel Comput* 33:541–560. <https://doi.org/10.1016/j.parco.2007.04.003>
- Esposti Ongaro T, Clarke AB, Neri A, Voight B, Widiwijayanti C (2008b) Fluid dynamics of the 1997 Boxing Day volcanic blast on Montserrat, West Indies. *J Geophys* 113:B03211–B03229. <https://doi.org/10.1029/2006JB004898>
- Esposti Ongaro T, Clarke AB, Voight B, Neri A, Widiwijayanti C (2012) Multiphase flow dynamics of pyroclastic density currents during the May 18, 1980 lateral blast of Mount St. Helens. *J Geophys Res* 117: B06208–B06222. <https://doi.org/10.1029/2011JB009081>
- Esposti Ongaro T, Cerminara M (2016) Non-equilibrium processes in ash-laden volcanic plumes: new insights from 3D multiphase flow simulations. *J Volcanol Geotherm Res* 326:127–142. <https://doi.org/10.1016/j.jvolgeores.2016.04.004>
- Esposti Ongaro, T., Komorowski, J.-C., Legendre, Y., Neri, A., 2020, Modelling pyroclastic density currents from a subplinian eruption at La Soufrière de Guadeloupe (West Indies, France). *Bull. Volcanol.*, 82:76, <https://doi.org/10.1007/s00445-020-01411-6>
- Feuillard M, Allègre CJ, Brandeis G, Gaulon R, Le Mouél JL, Mercier JC, Pozzi JP, Semet MP (1983) The 1975–1977 crisis of La Soufrière de Guadeloupe (F.W.I): a still-born magmatic eruption. *J Volcanol Geotherm Res* 16:317–334

Folch A., Costa A., Hankin R.K.S., 2009. TWODEE-2: A shallow layer model for dense gas dispersion on complex topography, *Comput. Geosci.*, doi:10.1016/j.cageo.2007.12.017

Global Volcanism Program (2019) Report on Stromboli (Italy). *Bull Global Volcanism Network* 44(9):3. <https://doi.org/10.5479/si.GVP.BGVN201909-211040>

Gurioli L, Pareschi MT, Zanella E, Lanza R, Deluca E, Bisson M (2005) Interaction of pyroclastic density currents with human settlements: evidence from ancient Pompeii. *Geol* 33:441–444. <https://doi.org/10.1130/G21294.1>

Hincks TK, Komorowski J-C, Sparks SR (2014) Retrospective analysis of uncertain eruption precursors at La Soufrière volcano, Guadeloupe, 1975–77: volcanic hazard assessment using a Bayesian Belief Network approach. *J Appl Volcanol* 3:3. <https://doi.org/10.1186/2191-5040-3-3>

Jenkins SF, Spence RJS, Fonseca JFBD, Solidum RU, Wilson TM (2010) Volcanic risk assessment: quantifying physical vulnerability in the built environment. *J Volcanol Geotherm Res* 276:105–120. <https://doi.org/10.1016/j.jvolgeores.2014.03.002>

Jenkins S, Komorowski J-C, Baxter PJ, Spence R, Picquout A, Lavigne F, Surono (2013a) The Merapi 2010 eruption: an interdisciplinary impact assessment methodology for studying pyroclastic density current dynamics. *J Volcanol Geotherm Res* 261:316–329. <https://doi.org/10.1016/j.jvolgeores.2013.02.012>

Jenkins S, Spence R, Baxter P, Komorowski J-C, Barsotti S, Esposti Ongaro T, Neri A (2013b) Modelling of disaster risk scenarios at La Soufrière, Guadeloupe. *Geophys Res Abstr* 15:EGU2013–EG10852

Jessop, D.E., Moune, S., Moretti, R., Gibert, D., Komorowski, J.-C., Robert, V., Heap, M.J., Bosson, A., Bonifacie, M., Deroussi, S., Dessert, C., Rosas-Carbal, M., Lemarchand, A., Burtin, A., 2021. A multi-decadal view of the heat and mass budget of a volcano in unrest: La Soufrière de Guadeloupe (French West Indies). *Bull. Volcanol*, 83:16. <https://doi.org/10.1007/s00445-021-01439-2>.

Jiménez, D., Becerril, L., Bartolini, S., & Martí, J. (2018). Spatio-temporal hazard estimation in San Miguel volcano, El Salvador. *Journal of Volcanology and Geothermal Research*, 358, 171–183. <https://doi.org/10.1016/j.jvolgeores.2018.04.003>

Kobes M, Helsloot I, De Vries B et al (2010) Way finding during fire evacuation; an analysis of unannounced fire drills in a hotel at night. *Build Environ* 45(3): 537–548. <https://doi.org/10.1016/j.buildenv.2009.07.004>

Komorowski J-C, Boudon G, Semet M, Beauducel F, Anténor-Habazac C, Bazin S, Hammouya G (2005) Volcanic Hazard Atlas of the Lesser Antilles: Guadeloupe. In: Lindsay J, Robertson R, Shepherd J, Ali S (eds) Volcanic Hazard Atlas of the Lesser Antilles, published by University of the West Indies. Seismic Research Unit, Trinidad and IAVCEI, pp 65–102

Komorowski J-C, Legendre Y., Caron B., Boudon G. (2008). Reconstruction and analysis of sub-Plinian tephra dispersal during the 1530 A.D. Soufrière (Guadeloupe) eruption: implications for scenario definition and hazards assessment *J. Volcanol. Geotherm. Res.* 178: 491-515

Komorowski J-C, Legendre Y, Boudon G et al (2012) A new Holocene eruptive chronology for La Soufrière of Guadeloupe volcano: implications for credible scenario definition as well as hazard and impact modelling. *Cities on Volcanoes* 7, 18-23 November 2012, IAVCEI, Colima, Mexico.

Komorowski, J-C, Legendre Y, Barsotti S (2013) Assessing long term hazards for La Soufrière of Guadeloupe volcano: insights from a new eruptive chronology, credible scenario definition, and integrated impact modelling. *International Association of Volcanology and Chemistry of the Earth's Interior (IAVCEI), Scientific Assembly, Kagoshima, Japan, 19-24 July 2013, abstract, 4W_4D-P1*

Komorowski, J.C., 2015. Maps from Institut de Physique du Globe de Paris, France (compiled and modified from Jolivet, 1958; Barrabé and Jolivet, 1958; Boudon et al., 1988; Komorowski et al., 2005; Feuillard, 2011, Legendre, 2012).

Lacanna G, Ripepe M. Tsunami wave by Pyroclastic flows recorded in near field, in preparation

- Legendre Y (2012) Reconstruction fine de l'histoire éruptive et scénarii éruptifs à La Soufrière de Guadeloupe: vers un modèle intégré de fonctionnement du volcan. PhD thesis, Institut de physique du globe de Paris, Université Paris Diderot, 1-430 pp, annexes 1-257 pp
- Leone F, Péroche M, Robustelli M et al (2018) Planifier les évacuations en cas de tsunami : la méthode EXPLOIT. Guide méthodologique. UMR GRED, Université Paul-Valéry 3 et IRD, p 73
- Leone F, Komorowski J-C, Gherardi-Leone M, Lalubie G (2019) Integrating spatial accessibility in the design of volcano evacuation plans in the French West Indies (Guadeloupe and Martinique). 1–22. doi: <https://doi.org/10.1186/s13617-019-0089-1>
- Ma J, Xu SM, Li T, Mu HL, Wen C, Song WG, Lo SM (2014) Method of bottleneck identification and evaluation during crowd evacuation process. *Proc Eng* 71: 454–461 <https://doi.org/10.1016/j.proeng.2014.04.065>
- Macedonio, G., Costa, A., Scollo, S., Neri, A., 2016. Effects of eruption source parameter variation and meteorological dataset on tephra fallout hazard assessment: example from Vesuvius (Italy). *Journal of Applied Volcanology*, 5(1), 1-19.
- Maramai A, Graziani L, Alessio G, Burrato P, Colini L, Cucci L, Nappi R, Nardi A, Vilardo G (2005) Near- and far-field survey report of the 30 December 2002 Stromboli (southern Italy) tsunami. *Mar Geol* 215(1-2):93–106. <https://doi.org/10.1016/j.margeo.2004.11.009>
- Massaro, S., Dioguardi, F., Sandri, L., Tamburello, G., Selva, J., Moune, S., Jessop, D.E., Moretti, R., Komorowski, J.-C., 2021. Testing gas dispersion modelling: A case study at La Soufrière volcano (Guadeloupe, Lesser Antilles), *Journal of Volcanology and Geothermal Research*, <https://doi.org/10.1016/j.jvolgeores.2021.107312>.
- Massaro S., Rossi, E., Sandri, L., Bonadonna, C., Selva, J., Moretti, R., Komorowski, J.-C. “Assessing hazard and impact associated with volcanic ballistic impacts: the example of La Soufrière de Guadeloupe volcano, Lesser Antilles”. Submitted to *Journal of Volcanology and Geothermal Research*.
- Moran SC, Newhall C, Roman DC (2011) Failed magmatic eruptions: late-stage cessation of magma ascent. *Bull Volcanol* 73:115–122. <https://doi.org/10.1007/s00445-010-0444-x>
- Moretti R, Komorowski J-C, Ucciani G, Moune S, Jessop D, de Chabaliér JB, Beauducel F, Bonifacie M, Burtin A, Vallée M, Deroussi S, Robert V, Gibert D, Didier T, Kitou T, Feuillet N, Allard P, Tamburello G, Shreve T, Saurel JM, Lemarchand A, Rosas-Carbajal M, Agrinier P, le Friant A, Chaussidon M (2020) The 2018 unrest phase at La Soufrière of Guadeloupe (French West Indies) andesitic volcano: scrutiny of a failed but prodromal phreatic eruption. *J Volcanol Geotherm Res* 393:106769. <https://doi.org/10.1016/j.jvolgeores.2020.106769>
- Nakano Y (2010) Design load evaluation for tsunami shelters based on damage observations after Indian ocean Tsunami disaster due to the 2004 Sumatra Earthquake. *Sci Tsunami Hazards* (25):13:.. <https://doi.org/10.3130/aijt.13.337-340>
- Neri A, Esposti Ongaro T, Macedonio G, Gidaspow S (2003) Multiparticle simulation of collapsing volcanic columns and pyro- clastic flow. *J Geophys Res* 108:2202–2224. <https://doi.org/10.1029/2001JB000508>
- OVSG-IPGP (1999-2020) Monthly report on the volcanic activity of La Soufrière de Guadeloupe and on the regional seismicity”, Observatoire Volcanologique et Sismologique de la Guadeloupe, Institut de physique du globe de Paris, IPGP-CNRS-INSU, Conseil Général de Guadeloupe. Published online at: <http://www.ipgp.fr/fr/ovsg/bulletins-mensuels-de-lovsg>; ISSN 1622-4523
- Péroche M (2016) La gestion de crise tsunami dans la Caraïbe : contribution géographique aux dispositifs d'alerte et d'évacuation des populations. Thèse de doctorat, p 407

- Peruzzetto M, Komorowski J-C, Le Friant A et al (2019) Modeling of partial dome collapse of La Soufrière of Guadeloupe volcano: implications for hazard assessment and monitoring. *Sci Rep Nature Publishing Group* 9:1–15. <https://doi.org/10.1038/s41598-019-49507-0>
- Pichavant M, Poussineau S, Lesne P, Solaro C, Bourdier J-L (2018) Experimental parametrization of magma mixing: application to the CE 1530 eruption of La Soufrière de Guadeloupe (Lesser Antilles). *J Petrol* 59(2):257–282
- Préfet de la Région Guadeloupe (2019) Arrêté N. 971-2019-01-14-006 du 14 janvier 2019 relatif à l'arrêté instituant un accès réglementé au sommet du volcan de la Soufrière (in French). <http://www.guadeloupe.gouv.fr/content/download/15905/103671/file/Arr%C3%AAt%C3%A9%20du%2014%20janvier%202019%20instituant%20un%20acc%C3%A8s%20r%C3%A9glement%C3%A9%20au%20sommet%20du%20volcan%20de%20la%20Soufrière%20C3%A8re.pdf>
- Rosas-Carbajal M, Komorowski J-C, Nicollin F, Gibert D (2016) Volcano electrical tomography unveils edifice collapse hazard linked to hydrothermal system structure and dynamics. *Sci Rep*:1–11. <https://doi.org/10.1038/srep29899>
- Sandri, L., Costa, A., Selva, J., Tonini, R., Macedonio, G., Folch, A., and Sulpizio, R. 2016. Beyond eruptive scenarios: assessing tephra fallout hazard from Neapolitan volcanoes. *Scientific Reports*, 6, 24271.
- Scarlato, P., Mollo, S., Del Bello, E., Von Quadt, A., Brown, R.J., Gutierrez, E., Martinez- Hackert, B., Papale, P. (2016). The 2013 eruption of Chaparrastique volcano (El Salvador): effects of magma storage, mixing, and decompression. *Chem. Geol.* 448, 110–122. <https://doi.org/10.1016/j.chemgeo.2016.11.015>
- Selva, J., Orsi, G., Di Vito, M. A., Marzocchi, W., and Sandri, L., 2012. Probability hazard map for future vent opening at the Campi Flegrei caldera, Italy. *Bull. Volcanol.*, 74(2), 497-510.
- Selva J., Costa A., De Natale G., Di Vito M.A., Isaia R., Macedonio G., 2018. Sensitivity test and ensemble hazard assessment for tephra fallout at Campi Flegrei, Italy. *J. Volcanol. Geotherm. Res.*, 351, 1-28, DOI:10.1016/j.jvolgeores.2017.11.024.
- Sobradelo, R., Bartolini, S., & Martí, J. (2013). HASSET: a probability event tree tool to evaluate future volcanic scenarios using Bayesian inference. *Bulletin of Volcanology*, 76(1), 770. <https://doi.org/10.1007/s00445-013-0770-x>
- Sobradelo, R. and Martí, J.: Short-term volcanic hazard assessment through Bayesian inference: Retrospective application to the Pinatubo 1991 volcanic crisis, *J. Volcanol. Geoth. Res.*, 290, 1–11, 2015.
- Spence, R., Komorowski, J.C., Saito, K., Brown, A., Pomonis, A., Toyos, G., and Baxter, P., 2008. Modelling the impact of a hypothetical sub-Plinian eruption at La Soufrière of Guadeloupe (Lesser Antilles). *J. Volcanol. Geotherm. Res.*, 178(3), 516-528.
- Suzuki YJ, Costa A, Cerminara M, Esposti Ongaro T, Herzog M, van Eaton AR, Denby LC (2016) Inter-comparison of three-dimensional models of volcanic plumes. *J Volcanol Geotherm Res* 326:26–42. <https://doi.org/10.1016/j.jvolgeores.2016.06.011>
- Tamburello, G., Moune, S., Allard, P., Venugopal, S., Robert, V., Rosas-Carbajal, M., Deroussi, Gaëtan-Thierry Kitou, Didier, T., Komorowski, J.C., Beauducel, F., De Chabaliér J.B., Le Marchand, A., Le Friant, A., Bonifacie, M., Dessert, C., and Moretti, R., 2019. Spatio-Temporal Relationships between Fumarolic Activity, Hydrothermal Fluid Circulation and Geophysical Signals at an Arc Volcano in Degassing Unrest: La Soufrière of Guadeloupe (French West Indies). *Geosciences*, 9(11), 480.
- Tierz, P., Sandri, L., Costa, A., Zaccarelli, L., Di Vito, M. A., Sulpizio, R., and Marzocchi, W., 2016. Suitability of energy cone for probabilistic volcanic hazard assessment: Validation tests at Somma-Vesuvius and Campi Flegrei (Italy). *Bull. Volcanol.*, 78, 79–92. <https://doi.org/10.1007/s00445-016-1073-9>.

-
- Tinti S, Maramai A, Armigliato A, Graziani L, Manucci A, Pagnoni G, Zaniboni F (2006a) Observations of physical effects from tsunamis of December 30, 2002 at Stromboli volcano, southern Italy. *Bull Volcanol* 68(5):450–461. <https://doi.org/10.1007/s00445-005-0021-x>
- Tinti S, Pagnoni G, Zaniboni F (2006b) The landslides and tsunamis of the 30th of December 2002 in Stromboli analysed through numerical simulations. *Bull Volcanol* 68(5):462–479. <https://doi.org/10.1007/s00445-005-0022-9>
- Trolese M, Cerminara M, Esposti Ongaro T, Giordano G (2019) The footprint of column collapse regimes on pyroclastic flow temperatures and plume heights. *Nat Commun* 10:2476. <https://doi.org/10.1038/s41467-019-10337-3>
- Villemant B., Komorowski, J.-C., Dessert C., Michel A., Crispi O., Hammouya G., Beauducel F., De Chabalier, (2014). Evidence for a new shallow magma intrusion at La Soufrière of Guadeloupe (Lesser Antilles). Insights from long-term geochemical monitoring of halogen-rich hydrothermal fluids. *Jour. Volcanol. Geotherm. Res.* 285, 247–277, doi: 10.1016/j.jvolgeores.2014.08.002
- Wang WL, Liu SB, Lo SM, Gao LJ (2014) Passenger ship evacuation simulation and validation by experimental data sets. *Proc Eng* 71:427–432 <https://doi.org/10.1016/j.proeng.2014.04.061>
- Williams, G.T., Kennedy, B.M., Wilson, T.M., Fitzgerald, R.H., Tsunematsu, K., and Teissier, A., 2017. Buildings vs. ballistics: Quantifying the vulnerability of buildings to volcanic ballistic impacts using field studies and pneumatic cannon experiments. *J. Volcanol. Geotherm. Res.* 343, 171–180.
- Wilson L, Sparks R, Walker GPL (1980) Explosive volcanic eruptions—IV. The control of magma properties and conduit geometry on eruption column behaviour. *Geophys J Int* 63:117–148. <https://doi.org/10.1111/j.1365-246x.1980.tb02613.x>

Appendix A: Links to concrete results

Published papers:

<https://doi.org/10.1016/j.jvolgeores.2021.107312>

<https://doi.org/10.1007/s00445-020-01411-6> <https://link.springer.com/article/10.1007/s00445-020-01411-6>

<https://doi.org/10.1007/s00445-020-01395-3>

<https://doi.org/10.1186/s13617-021-00104-9>

Journal of Volcanology and Geothermal Research 417 (2021) 107312



Testing gas dispersion modelling: A case study at La Soufrière volcano (Guadeloupe, Lesser Antilles)



Silvia Massaro^{a,b,*}, Fabio Dioguardi^c, Laura Sandri^a, Giancarlo Tamburello^a, Jacopo Selva^a, Séverine Moune^{d,e,f}, David E. Jessop^{d,e,f}, Roberto Moretti^{d,e}, Jean-Christophe Komorowski^d, Antonio Costa^a

^a Istituto Nazionale di Geofisica e Vulcanologia, Sezione di Bologna, Italia

^b Istituto di Geologia Ambientale e Geoingegneria, Consiglio Nazionale delle Ricerche, Area di Ricerca Roma 1, Sede Montelibretti, Italia

^c British Geological Survey, The Lyell Centre, Edinburgh, United Kingdom

^d Université de Paris, Institut de Physique du Globe de Paris, UMR CNRS 7154, Paris, France

^e Observatoire Volcanologique et Sismologique de Guadeloupe, Institut de Physique du Globe de Paris, Gourbeyre, Guadeloupe

^f Université Clermont Auvergne, CNRS, IRD, OPGC Laboratoire Magmas et Volcans, F-63000 Clermont-Ferrand, France

ARTICLE INFO

Article history:

Received 18 November 2020

Received in revised form 5 June 2021

Accepted 9 June 2021

Available online 11 June 2021

Keywords:

Passive gas dispersion

Numerical modelling

ERA5 reanalysis

Mass consistent wind model

La Soufrière de Guadeloupe

ABSTRACT

Volcanic gas dispersal can be a serious threat to people living near active volcanoes since it can have short- and long-term effects on human health, and severely damage crops and agricultural land. In recent decades, reliable computational models have significantly advanced, and now they may represent a valuable tool to make quantitative and testable predictions, supporting gas dispersal forecasting and hazard assessments for public safety. Before applying a specific modelling tool into hazard quantification, its calibration and its sensitivity to initial and boundary conditions should be carefully tested against available data, in order to produce unbiased hazard quantifications. In this study, we provided a number of prototypical tests aimed to validate the modelling of gas dispersal from a hazard perspective. The tests were carried out at La Soufrière de Guadeloupe volcano, one of the most active gas emitters in the Lesser Antilles.

La Soufrière de Guadeloupe has shown quasi-permanent degassing of a low-temperature hydrothermal nature since its last magmatic eruption in 1530 CE, when the current dome was emplaced. We focused on the distribution of CO₂ and H₂S discharged from the three main present-day fumarolic sources at the summit, using the measurements of continuous gas concentrations collected in the period March–April 2017. We developed a new probabilistic implementation of the Eulerian code DISGAS-2.0 for passive gas dispersion coupled with the mass-consistent Diagnostic Wind Model, using local wind measurements and atmospheric stability information from a local meteorological station and ERA5 reanalysis data. We found that model outputs were not significantly affected by the type of wind data but rather upon the relative positions of fumaroles and measurement stations. Our results reproduced the statistical variability in daily averages of observed data over the investigated period within acceptable ranges, indicating the potential usefulness of DISGAS-2.0 as a tool for reproducing the observed fumarolic degassing and for quantifying gas hazard at La Soufrière. The adopted testing procedure allows for an aware application of simulation tools for quantifying the hazard, and thus we think that this kind of testing should actually be the first logical step to be taken when applying a simulator to assess (gas) hazard in any other volcanic contexts.

© 2021 The Authors. Published by Elsevier B.V. This is an open access article under the CC BY-NC-ND license (<http://creativecommons.org/licenses/by-nc-nd/4.0/>).

1. Introduction

Volcanic gases are mixtures of volatile compounds generated by magmas exsolving volatiles at low pressures during their ascent and storage near the surface. The solubilities of volatile components demand that gas compositions are dominated by the more melt-soluble components (such as H₂O, SO₂ and halogens), with CO₂ solubility decreases as

magma decompresses and ascends up to the surface. However, even for open-conduit-volcano, processes are more complicated than this simple sketch. On one hand, depending on the state of the volcano and its internal dynamics, volcanic gas compositions sum-up the degassing from shallow magma and the deeper portions of the plumbing system, down to the magma chamber (e.g., Symonds, 1994; Oppenheimer et al., 2011; Moretti et al., 2013; Aiuppa et al., 2007, 2010, 2016, 2017a; Erfurt-Cooper, 2018). On the other hand, at closed-conduit and generally andesitic volcanoes, we observe focused vents (fumaroles) releasing in atmosphere steam-rich (>90% vol; e.g., Giggenbach, 1996) compositions that reflect the sharp physico-chemical change from the

* Corresponding author at: Istituto Nazionale di Geofisica e Vulcanologia, Sezione di Bologna, Italia.

E-mail addresses: silvia.massaro@ingv.it, silvia.massaro@igag.cnr.it (S. Massaro).

<https://doi.org/10.1016/j.jvolgeores.2021.107312>

0377-0273/© 2021 The Authors. Published by Elsevier B.V. This is an open access article under the CC BY-NC-ND license (<http://creativecommons.org/licenses/by-nc-nd/4.0/>).

Figure A.1. Front page of the paper Massaro, S., Dioguardi, F., Sandri, L., Tamburello, G., Selva, J., Moune, S., Jessop, D.E., Moretti, R., Komorowski, J.-C., Costa, A., 2021 “Testing gas dispersion modelling: A case study at La Soufrière volcano (Guadeloupe, Lesser Antilles)”, Journal of Volcanology and Geothermal Research, 417, 107312, <https://doi.org/10.1016/j.jvolgeores.2021.107312>



Modelling pyroclastic density currents from a subplinian eruption at La Soufrière de Guadeloupe (West Indies, France)

Tomaso Esposti Ongaro¹ · Jean-Christophe Komorowski² · Yoann Legendre³ · Augusto Neri¹

Received: 29 February 2020 / Accepted: 1 October 2020
 © The Author(s) 2020

Abstract

We have used a three-dimensional, non-equilibrium multiphase flow numerical model to simulate subplinian eruption scenarios at La Soufrière de Guadeloupe (Lesser Antilles, France). Initial and boundary conditions for computer simulations were set on the basis of independent estimates of eruption source parameters (i.e. mass eruption rate, volatile content, temperature, grain size distribution) from a field reconstruction of the 1530 CE subplinian eruption. This event is here taken as a reference scenario for hazard assessment at La Soufrière de Guadeloupe. A parametric study on eruption source parameters allowed us to quantify their influence on the simulated dynamics and, in particular, the increase of the percentage of column collapse and pyroclastic density current (PDC) intensity, at constant mass eruption rate, with variable vent diameter. Numerical results enabled us to quantify the effects of the proximal morphology on distributing the collapsing mass around the volcano and into deep and long valleys and to estimate the areas invaded by PDCs, their associated temperature and dynamic pressure. Significant impact (temperature > 300 °C and dynamic pressure > 1 kPa) in the inhabited region around the volcano is expected for fully collapsing conditions and mass eruption rates > 2×10^7 kg/s. We thus combine this spatial distribution of temperature and dynamic pressure with an objective consideration of model-related uncertainty to produce preliminary PDC hazard maps for the reference scenario. In such a representation, we identify three areas of varying degree of susceptibility to invasion by PDCs—very likely to be invaded (and highly impacted), susceptible to invasion (and moderately impacted), and unlikely to be invaded (or marginally impacted). The study also raises some key questions about the use of deterministic scenario simulations for hazard assessment, where probability distributions and uncertainties are difficult to estimate. Use of high-performance computing techniques will in part allow us to overcome such difficulties, but the problem remains open in a scientific context where validation of numerical models is still, necessarily, an incomplete and ongoing process. Nevertheless, our findings provide an important contribution to the quantitative assessment of volcanic hazard and risk at La Soufrière de Guadeloupe particularly in the context of the current unrest of the volcano and the need to prepare for a possible future reawakening of the volcano that could culminate in a magmatic explosive eruption.

Keywords La Soufrière de Guadeloupe · Pyroclastic density currents · Subplinian eruption · Numerical simulation · Hazard assessment

Editorial responsibility: C.E.Gregg

✉ Tomaso Esposti Ongaro
tomaso.espostiongaro@ingv.it

¹ Istituto Nazionale di Geofisica e Vulcanologia (INGV), Sezione di Pisa, Italy

² Université de Paris, Institut de Physique du Globe de Paris (IPGP), CNRS, Paris, France

³ Bureau de Recherches Géologiques et Minières (BRGM), Petit-Bourg, Guadeloupe, France

Published online: 13 November 2020



Introduction

Pyroclastic density currents are rapidly moving, gravity-driven flows of gas and hot volcanic particles (ash, lapilli, and blocks) produced during explosive eruptions (Sparks et al. 1978; Druitt 1998; Branney and Kokelaar 2002). They represent extreme hazards at active volcanoes by virtue of their rapid propagation, attaining velocities of up to 60 m/s (e.g. Yamamoto et al. 1993; Loughlin et al. 2002; Komorowski et al. 2015), destructive potential (Spence et al. 2004; Baxter et al. 2005; Jenkins et al. 2010, 2013a), and for the lethal conditions rapidly establishing in the inundated areas (Baxter et al. 2017). Assessing PDC hazards and their

Figure A.2. Front page of the paper: Esposti Ongaro, T., Komorowski, J-C., Legendre, Y., Neri, A., 2020, *Modelling pyroclastic density currents from a subplinian eruption at La Soufrière de Guadeloupe (West Indies, France)*. Bulletin of Volcanology, 82:76, <https://link.springer.com/article/10.1007/s00445-020-01411-6>

Research Article | Published: 20 June 2020

Probabilistic hazard maps for operational use: the case of SO₂ air pollution during the Holuhraun eruption (Bárðarbunga, Iceland) in 2014–2015

Sara Barsotti 

Bulletin of Volcanology **82**, Article number: 56 (2020) | [Cite this article](#)

1238 Accesses | **1** Citations | [Metrics](#)

Abstract

The Holuhraun fissure eruption (Iceland) in 2014–2015, which originated from the Bárðarbunga volcanic system, was exceptional in several respects. It lasted 6 months and, throughout its duration, it released up to 9.6 Mt of SO₂ in the atmosphere. The main recorded hazard affecting the entire country over the 6 months was the constant presence of a low-level gas cloud that led to recurrent air pollution episodes. The Icelandic Meteorological Office responded to this human health hazard by (1) setting up a forecasting system to anticipate the distribution of SO₂ over Iceland and (2) preparing probabilistic hazard maps to support the decisions taken by the Icelandic Civil Protection in demarcating the accessible area around the eruption site. This paper introduces some technical aspects of the application of the CALPUFF numerical model to this eruption like the SO₂ dispersal forecasting setup, the volcanic source numerical description, and the Monte Carlo procedure adopted for the creation of the probabilistic hazard maps. CALPUFF-based maps were created in January 2015, when the


Figure A.3. Front page of the paper Barsotti, S 2020. Probabilistic hazard maps for operational use: the case of SO₂ air pollution during the Holuhraun eruption (Bárðarbunga, Iceland) in 2014–2015. *Bull Volcanol* **82**, 56 (2020). <https://doi.org/10.1007/s00445-020-01395-3>

RESEARCH

Open Access



Tsunami evacuation times and routes to safe zones: a GIS-based approach to tsunami evacuation planning on the island of Stromboli, Italy

Emmie M. Bonilauri¹ , Andrew J. L. Harris^{1*}, Julie Morin^{1,2}, Maurizio Ripepe³, Domenico Mangione⁴, Giorgio Lacanna³, Stefano Ciolli⁴, Maria Cusolito⁵ and Pauline Deguy⁶

Abstract

While a landslide at the volcanic island of Stromboli (Aeolian Islands, Italy) in December 2002 created a tsunami with a run-up of 10.9 m, two paroxysmal eruptions in the summer of 2019 caused a tsunami with an amplitude of 40 to 20 cm. All three events required rapid, spontaneous emergency evacuations of the beach zone as the time between tsunami generation and impact is around 4 min. These conditions thus require a special consideration of the issue of evacuation capabilities on the island in the event of a volcanogenic tsunami. The purpose of this paper is thus to (i) determine pedestrian evacuation times from high-risk coastal areas to safe zones, (ii) to assess building evacuation ease, and (iii) determine emergency evacuation plans (for buildings and coastal zones). For this purpose, we created a GIS-based risk analysis/mapping tool that also allowed macroscopic evacuation modelling. In our case, the high-risk zone to be evacuated involves an area extending to 10 m a.s.l. and involving 123 individual buildings over an area of 0.18 km². The results show that 33% of the buildings can be evacuated in 4 min, and that a 10-min warning time is required for a complete and well-distributed evacuation whereby the population is evenly distributed between all evacuation exits to avoid the potential for congestion. Initial interviews of residents in the at-risk zone reveal a high level of awareness and a desire for personalized evacuation scenarios.

Keywords: Stromboli, Volcanogenic tsunami, Volcanic island hazard, Evacuation modelling, Evacuation maps

Introduction

All international tsunami risk management bodies agree that planning for evacuation drastically reduces the risk and saves lives among coastal populations (Scheer et al. 2011; FEMA 2019). Evacuation plans allow for effective placement of signs indicating danger zones, refuge sites, and evacuation routes (Dall'Osso and Dominey-Howes 2010; FEMA 2019) and can be used to support increased public

awareness, which will help to develop reflexes and resilience of coastal populations (Gregg et al. 2006; Kelman et al. 2008; Morin et al. 2008; Løvholt et al. 2019; Wood et al. 2019), improving the efficiency of future evacuations (Péroche 2016). A number of studies have been carried out around the world to reduce the impact of tsunamis on populations by increasing the efficiency of evacuations through planning (Lämmel et al. 2010; Sahal 2011; Leone et al. 2013, 2014, 2018; Péroche et al. 2014; Péroche 2016). What all of these studies show is that an effective evacuation has to be based on a viable plan that takes into account the physical state of evacuation routes

* Correspondence: Andrew.HARRIS@uca.fr

¹Université Clermont Auvergne, CNRS, IRD, OPGC, Laboratoire Magmas et Volcans, Clermont – Ferrand, France

Full list of author information is available at the end of the article



© The Author(s). 2021 **Open Access** This article is licensed under a Creative Commons Attribution 4.0 International License, which permits use, sharing, adaptation, distribution and reproduction in any medium or format, as long as you give appropriate credit to the original author(s) and the source, provide a link to the Creative Commons licence, and indicate if changes were made. The images or other third party material in this article are included in the article's Creative Commons licence, unless indicated otherwise in a credit line to the material. If material is not included in the article's Creative Commons licence and your intended use is not permitted by statutory regulation or exceeds the permitted use, you will need to obtain permission directly from the copyright holder. To view a copy of this licence, visit <http://creativecommons.org/licenses/by/4.0/>. The Creative Commons Public Domain Dedication waiver (<http://creativecommons.org/publicdomain/zero/1.0/>) applies to the data made available in this article, unless otherwise stated in a credit line to the data.

Figure A.4. Front page of the paper Bonilauri E, Harris A, Morin J, et al., 2021. Tsunami evacuation times and routes to safe zones: a GIS-based approach to tsunami evacuation planning on the island of Stromboli, Italy. *Journal of Applied Volcanology* 10:4. <https://doi.org/10.1186/s13617-021-00104-9>